THESIS

TECHNO-ECONOMIC ANALYSIS AND LIFE CYCLE ASSESSMENT OF ALGAL TURF SCRUBBERS TREATING ANAEROBIC LAGOON EFFLUENT FOR NUTRIENT RECOVERY AND RENEWABLE DIESEL PRODUCTION

Submitted by

Luis Triminio

Department of Mechanical Engineering

In partial fulfillment of the requirements

For the Degree of Master of Science

Colorado State University

Fort Collins, Colorado

Summer 2026

Master's Committee:

Advisor: Jason Quinn

Bret Windom
Kenneth Reardon

ABSTRACT

TECHNO-ECONOMIC ANALYSIS AND LIFE CYCLE ASSESSMENT OF ALGAL TURF SCRUBBERS TREATING ANAEROBIC LAGOON EFFLUENT FOR NUTRIENT RECOVERY AND RENEWABLE DIESEL PRODUCTION

High-nutrient wastewater sources, such as anaerobic dairy lagoon effluent, contribute to nitrogen (N) and phosphorus (P) overapplication, groundwater contamination, and surface-water impairment. Algal turf scrubbers (ATS) can recover these nutrients while producing harvestable biomass for bioproducts, but the economic feasibility of treatment remains unexplored. This study presents the first national-scale techno-economic and life cycle assessment of a modular ATS system for treating dairy anaerobic lagoon effluent across the contiguous United States, using a county-level model informed by 2022 dairy census data, manure-management datasets, and process wastewater criteria. Nutrient removal was simulated using an experimentally validated framework integrating Monod-based biokinetics and light-use-efficiency-based biomass productivity. Harvested biomass was routed to centralized state-level hydrothermal liquefaction facilities for renewable diesel production. Results show that ATS-derived renewable diesel remained economically challenging, with fuel selling prices exceeding the U.S. average fuel selling price of \$0.98 LGE^{-1} across all cost assumptions. However, to reach economic parity, the required nutrient credits were below conventional treatment cost benchmarks for 30-96% of locations for N and 65-96% for P, depending on cost assumptions. For wastewater treatment alone, lower cultivation-cost assumptions allowed 94% of evaluated locations to fall below a \$1.61 m^{-3} treatment benchmark. Life-cycle results showed that most locations exceeded low-carbon fuel

thresholds due to cultivation and biomass transportation burdens. Overall, while ATS-derived renewable diesel faces persistent economic and carbon-intensity barriers, lagoon-based ATS systems demonstrate strong potential as a nutrient-recovery technology with potential fuel co-production serving as a supplementary benefit rather than a primary value driver.

ACKNOWLEDGEMENTS

The author gratefully acknowledges financial support from the United States Department of Energy (DE0010293). Special thanks are extended to Peter Chen, Ashley Ryland and Owen Adams at the Powerhouse Energy Institute for assisting with the experimental work that supported this study. The author would also like to acknowledge Sungwhan Kim, Ryan Davis and Tyler Eckles from Sandia National Laboratories; Sybil Sharvelle and Kenneth F. Reardon from Colorado State University for their technical bio-chemical expertise; and Mark Zivojnovich for his insights on commercial-scale implementation. Gratitude is further extended to Jason Quinn, Jonah M. Greene and the members of the Sustainability Research Lab at the Powerhouse Energy Institute for their ongoing support throughout this work. Finally, I would like to thank David Quiroz Nuila from Ohio University for his support and guidance throughout this work, from the first day to the final manuscript of this paper.

TABLE OF CONTENTS

1. INTRODUCTION

Manure management is both a water-quality and greenhouse gas emissions (GHG) challenge in dairy production. Dairy operations rely on manure storage and land application to manage large volumes of wastewater, nutrients, and organic matter; however, these systems can contribute to nutrient overloading in surrounding water bodies through runoff and leaching. Globally, livestock manure contained approximately 125 million metric tons (MMT) of nitrogen (N) in 2018, with about 20 MMT released to the atmosphere and 35 MMT leached into aquifers and surface water bodies [1]. In the United States, manure management contributed approximately 81.7 MMT of carbon dioxide equivalent (CO_{2e}) in 2022, including 64.7 MMT from methane (CH_4) and 17.0 MMT from nitrous oxide (N_2O) [2]. These nutrient losses contribute to groundwater contamination, surface-water eutrophication, and degradation of receiving water bodies, while manure-derived emissions remain an important environmental concern. Together, these challenges highlight the need for treatment strategies that improve nutrient recovery and reduce water-quality risks associated with dairy wastewater management [1], [2].

Manure waste management technologies, including anaerobic digestion [3], anaerobic lagoons, and associated biogas recovery systems, have expanded in recent years to reduce emissions and recover value from organic waste streams [4], [5]. However, water and nutrient management remain persistent challenges in livestock systems [6]. Biological treatment of manure wastewater can occur under aerobic or anaerobic conditions. Aerobic systems can oxidize organic carbon and reduce odor formation, but treating high-strength dairy manure aerobically requires substantial aeration, infrastructure, and operating costs [7]. Consequently, anaerobic systems remain a practical and cost-effective option for livestock operations. As described by the Natural

Resources Conservation Service (NRCS), anaerobic lagoons are engineered earthen impoundments designed to treat and store manure wastewater by stabilizing organic matter, reducing pollution potential, and protecting water quality [8]. However, this treatment does not fully eliminate environmental concerns: organic matter degradation can generate odors through volatile fatty acid accumulation, while lagoon effluent can retain elevated N and P concentrations that contribute to ammonia NH_3 volatilization, leaching, runoff, and residual nutrient discharge [8], [9]. In dairy systems, water commonly flushes manure from barns to anaerobic lagoons. After treatment and storage, lagoon effluent is typically applied to grass, corn silage, forage, or other non-human-consumption crops for irrigation and nutrient supply [10], [11]. This management pathway creates an opportunity for nutrient-recovery treatment before land application, reducing reliance on storage, dilution, and crop uptake alone [7], [11].

Algal Turf Scrubber® (ATS™) systems are an attractive treatment platform in which nutrient-rich water is intermittently pulsed across shallow, sloped flow-ways to support the cultivation of dense periphytic algal communities. These algal biofilms assimilate N and phosphorus (P) into harvestable biomass that can be used for bioproducts while improving water quality [12]. ATS systems have been deployed at pilot scale across multiple sites in the United States and evaluated for dairy wastewater treatment in previous studies [13], [14], [15], [16]. These studies demonstrate the potential of ATS systems to improve effluent quality and recover biomass from nutrient-rich wastewater streams. Beyond nutrient recovery, harvested ATS biomass can serve as a feedstock for thermochemical conversion pathways such as hydrothermal liquefaction (HTL). HTL is particularly attractive because it can process wet biomass without energy-intensive drying, producing biocrude that can be upgraded into renewable diesel [17], [18]. Thus, coupling

ATS with HTL links lagoon effluent treatment, nutrient recovery, biomass production, and renewable fuel generation.

Previous studies have evaluated the economic and environmental performance of ATS-based wastewater treatment [19], [20] and HTL systems [21]. Among these studies, Ryland et al. [19] evaluated ATS treatment of wastewater treatment plant effluent and incorporated nutrient credits, which assign an economic value to N and P removal based on the avoided cost of achieving comparable nutrient reductions with conventional treatment technologies. Banks et al. [20] evaluated ATS deployment for surface water treatment, demonstrating its potential for nutrient removal and biomass recovery. These assessments have focused more on dilute wastewater sources with N concentrations of 0-20 mg N L^{-1} and P concentrations of 0-5 mg P L^{-1}, whereas anaerobic lagoon effluent represents a more concentrated nutrient stream of 730 mgN L^{-1} and 160 mgP L^{-1} [22] that may influence hydraulic design and system scale-up requirements. Therefore, a more detailed assessment is needed to evaluate ATS-HTL integration under dairy lagoon conditions by considering regional wastewater availability, cultivation system sizing, biomass production, and renewable diesel conversion within a unified techno-economic and environmental framework [16], [23].

In addition, high-nutrient algal treatment studies, including Mulbry et al. [23], [24], have shown that the rate of N and P recovery is strongly linked to harvested biomass, but higher nutrient loading can increase the importance of non-biomass removal mechanisms. Under dairy lagoon conditions, nutrient concentrations may exceed the immediate assimilation capacity of algal biomass, requiring consideration of ammonia volatilization, nitrification-denitrification, phosphorus precipitation or sorption, settling, and microbial immobilization [25], [26]. In the context of economic feasibility, these pathways influence nutrient-credit value, biomass available for HTL conversion, treatment emissions, and system sizing. Therefore, anaerobic lagoon effluent requires a modeling framework that separates biomass-based uptake from other removal mechanisms while accounting for recirculation time, treatment area, and concentration-dependent kinetics using Monod-based relationships, which describe how microbial nutrient uptake rates vary with substrate concentration. Recirculation and residence time determine effluent-biofilm contact and nutrient removal, while treatment area controls biomass production, land requirements, and capital cost.

Building on this prior work, this study developed an integrated spatial modeling framework that combines anaerobic lagoon nutrient concentrations, Monod-based uptake kinetics, modular ATS design, county-level dairy wastewater availability across the contiguous United States (CONUS), and centralized HTL conversion. The framework integrates dairy census data, manure-management modeling, process wastewater criteria, and regional productivity constraints to estimate nutrient removal, biomass production, renewable diesel output, and associated economic and environmental performance. This work addresses three key gaps: evaluating ATS biomass from dairy lagoon locations as a renewable diesel feedstock, assessing ATS performance under high-nutrient lagoon conditions rather than dilute wastewater sources, and incorporating biokinetic modeling to account for biomass-based and additional nutrient removal pathways. By connecting wastewater treatment, nutrient recovery, and fuel production in a spatially resolved framework, this study evaluates whether ATS systems can provide water-quality benefits while supporting renewable diesel production from dairy lagoon effluent.

2. METHODOLOGY

This study evaluated an integrated pathway from ATS-based wastewater treatment to renewable diesel production through HTL. A modular process model quantified mass and energy flows for an ATS facility treating anaerobic lagoon effluent, and model outputs were used for techno-economic analysis (TEA) and life-cycle assessment (LCA). The following sections describe the process model (Section 2.1), dairy lagoon flow and nutrient inventory (Section 2.2), ATS productivity and nutrient-removal model (Section 2.3), design constraints and system sizing (Section 2.4), HTL conversion model (Section 2.5), TEA (Section 2.6), LCA (Section 2.7), and sensitivity and uncertainty analyses (Section 2.8).

2.1 Process Model

2.1.1 System Boundary

The system boundary in Figure 1 encompassed ATS-based nutrient treatment of anaerobic lagoon effluent, recirculation and reuse of treated effluent, biomass harvesting and transport, ash reduction, biorefinery conversion to renewable diesel, fuel distribution, and combustion end-use. Required treatment area was estimated at the county level based on effluent flow, nutrient loading, and regional productivity. Manure conveyance by flush water, coarse fiber filtration, and anaerobic lagoon storage were treated as part of the business-as-usual process. Within the ATS system, algae assimilated N and P into harvestable biomass, while treated water passed through coarse fiber filtration and was stored for potential reuse on non-human consumption crops. When irrigation reuse was not required, treated water was recycled as flush water or used to dilute incoming manure to the target ATS influent concentration. Harvested algal biomass was routed to a centralized biorefinery for ash reduction, slurry adjustment to approximately 20% solids, HTL conversion to biocrude, and upgrading to renewable diesel. The system also included renewable diesel transport and combustion, pump and biorefinery energy use, displacement of conventional fertilizers including diammonium phosphate (DAP) and NH_3, process emissions of CO_2 and N_2O, and CO_2 uptake from biomass growth. Figure 1 summarizes the overall process flow and system boundary.

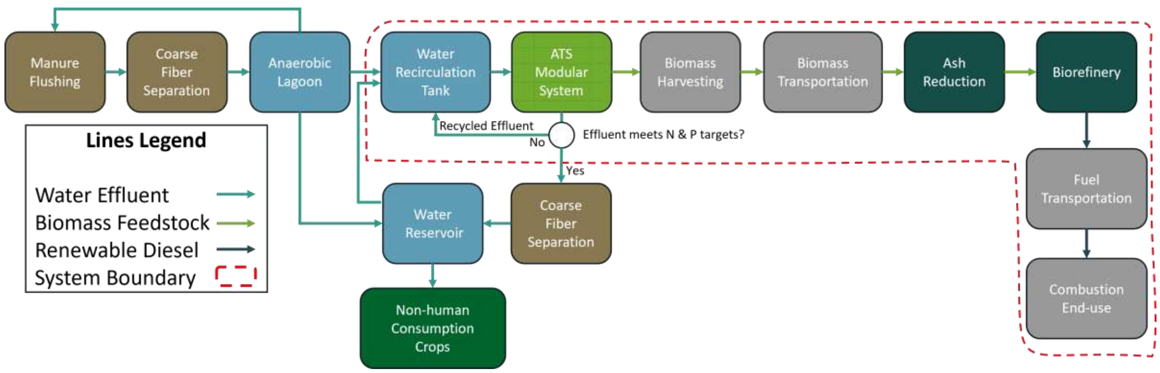

Figure 1. Process flow diagram and system boundary for ATS treatment of anaerobic lagoon effluent and renewable diesel production. Brown boxes represent manure-liquid streams, blue boxes represent water storage or treatment tanks, light green represents the modular ATS treatment system (experimentally validated), dark green represents non-human consumption crops, gray boxes represent fuel use for harvesting and transportation, and dark teal boxes represent biorefinery-related processes. The red dashed boundary indicates the processes system boundary, beginning with lagoon effluent extraction and ending with renewable diesel combustion.

Oxygen generated through algal photosynthesis, together with atmospheric oxygen transfer, was assumed to support nitrification within the ATS [22]. Under these aerobic conditions, ammonium (NH_4^+) was assumed to be oxidized to nitrate (NO_3^-) [27], consistent with laboratory observations that showed NH_3 consumed and nitrified within 1–3 days at initial concentrations of 50 and 100 ppm (Appendix Figure A12). Localized anoxic microenvironments within the algal biofilm were also assumed to support denitrification, producing N_2 and small amounts of N_2O [28].

Dairy lagoon effluent was not assumed to be transported to municipal wastewater treatment plants or treated to tertiary discharge quality because dairy farms are often distant from centralized facilities, and pipeline infrastructure would require separate economic justification [29]. Instead, treated effluent was assumed to be reused for irrigation of non-food crops, with ATS treatment reducing N and P concentrations to better align with crop demand and reduce nutrient overapplication risks [8], [11], [30], [31], [32]. Because the NRCS-based initial concentration of 730 ppm-N was outside validated pilot-scale ranges and potentially inhibitory to algae, influent wastewater was diluted to a maximum of 100 ppm-N while maintaining a 10:1 N:P ratio. Initial dilution was assumed to use purchased commercial water under outside-city-limits non-water-budget rates, after which treated ATS effluent was recycled as dilution water for subsequent batches. Water was assumed to recirculate continuously from the tank through the algal cultivation channels and return by gravity, with channels inclined at approximately 1°**.**

2.2 Dairy Lagoon Flow and Nutrient Target Inventory

The spatial boundary included potential anaerobic lagoon sites across the CONUS. Candidate sites were identified using USDA National Agricultural Statistics Service (NASS) Quick Stats dairy cattle data and screened using EPA Title 40 thresholds, where dairy operations with more than 200 cows are required to implement a manure or wastewater management system [33], [34]. This screening reduced 3,107 potential dairy locations to 830 viable dairy-lagoon sites. The ATS model then incorporated EPA manure-management data, including manure properties and state-level manure distribution fractions aligned with the 2022 USDA Census.

For each county, the number of dairy cows connected to anaerobic lagoons was estimated by multiplying the county-level dairy inventory by the state-level fraction of manure managed in anaerobic lagoons reported by EPA [35]. Wastewater flow was then calculated using the NRCS lagoon effluent factor of 234 lb cow^{-1} day^{-1} equivalent to approximately 106 L cow^{-1} day^{-1}[22] to estimate the daily wastewater inflow available for ATS treatment. This flow was combined with NRCS lagoon effluent characteristics of 2% total solids (TS), 0.073% total Kjeldahl nitrogen (TKN), and 0.016% phosphorus (P) to estimate annual total nitrogen (TN) and total phosphorus (TP) loads entering the ATS system (Appendix Section A3). Solids-related light attenuation was expected to be minimal because ATS systems operate as shallow thin-film flow-ways. Lagoon effluent also contains biological oxygen demand (BOD), with reported BOD_5 of 350 mg L^{-1} (2.92 lb per 1,000 gal) [22]. After dilution, this corresponds to approximately 48 mg L^{-1} BOD_5, indicating that heterotrophic microbial growth could occur. However, this contribution was not expected to dominate productivity relative to light-driven algal growth under the ATS conditions modeled in this study and was therefore excluded from the productivity model [36].

Crop nutrient targets for the ATS system were defined from crop nutrient demand and average irrigation depths. Nitrogen and phosphorus requirements for representative crops, including grass, corn silage, and forage systems, were obtained from Clark et al. [30]. Minimum, midpoint, and maximum nutrient-demand scenarios were developed from the reported range of crop yield goals, with higher yield goals corresponding to greater nutrient requirements. State-level USDA irrigation depths were then used to convert these area-based nutrient demands into equivalent concentration targets in applied water [37]. Preliminary screening showed that crop selection had less influence on optimal ATS sizing than productivity, cultivation cost, and operational days. Therefore, the grass-minimum case, defined as the lowest nutrient-demand scenario among the evaluated grass yield goals, was selected as the primary reuse scenario because it resulted in the lowest nutrient concentration targets in applied water, representing the most stringent treatment requirement and the most conservative assumption for ATS sizing and cost estimation.

2.3 ATS productivity experiments and nutrient-removal model

The indoor laboratory system at the Energy Institute at Colorado State University (CSU) consisted of two flow-ways operated at 50 and 100 ppm TN, both with a 10:1 N:P ratio, to evaluate algal growth under different nutrient loadings. Growth experiments were conducted to determine nutrient uptake dynamics using the experimental setup and algal biomass composition described by Ryland et al. [19]. Each flow-way had a water volume of 454 L, a flow-way cultivation area of 0.59 m^2, a constant pH of 8 ± 0.10, constant temperature of 28 ± 2 °C, constant air supply, and an average photosynthetically active radiation (PAR) of 708 μmol m^{-2} s^{-1} (GHI of 338 W m^{-2}) in a diurnal cycle. Biomass productivity was parameterized using county-level average GHI (Appendix Figure A3) and the experimentally derived light-use efficiency of 2.71 ± 0.57% (Appendix Figure A14), which is comparable to the 2.80% reported by Banks et al. [20]. Experimentally measured nutrient removal rates were then used to estimate N and P removal for each county-level ATS system. ATS operational days were restricted to the temperature-dependent operating window defined by Ryland et al. [19], with days excluded when the average daily ambient temperature was below 10 °C and therefore considered unsuitable for biomass production.

2.3.1 Experimental Nutrient Removal Rates

Water samples were collected daily from each flow-way over 12 weeks at the CSU Energy Institute to track TN and TP concentrations using HACH spectrophotometry (DR6000). Average removal rates were calculated from the initial concentration and the concentration measured on each harvest day, while the complete daily dataset was used to develop the biokinetic model. N and P removal rates per harvest were defined as follows, with additional details provided in Appendix Section A7:

$$\Delta S = S_i - S_f \ [\boldsymbol{Eq.1}]$$

$$R_s = \frac{\Delta S * V}{A * t} \ [\boldsymbol{Eq.2}]$$

where ΔS is the substrate removed (mg L^{-1}), S_i and S_f are the initial and final substrate concentrations (mg L^{-1}), V is the total volume (L), A is the algal cultivation area (m^2), t is time between harvests (days), and R_s is the substrate removal rate (mg substrate m^{-2} day^{-1}).

N and P removal rates were averaged across the experimental period to obtain representative mean values and standard deviations. Because high-nutrient systems may remove only 40-60% of N and P through algal assimilation, with the remainder attributed to microbial, settling, or physicochemical processes, total removal was separated into biomass-associated uptake and other removal pathways [12], [24]. Biomass-associated removal was estimated from measured productivity, sloughed biomass, and validated biomass composition, while the remaining fraction was calculated by difference and assigned to secondary removal mechanisms.

For non-assimilatory N removal, denitrification was treated as the microbial pathway represented in the model, while the remaining removal was assigned to other non-assimilatory pathways. Denitrification was assumed to account for approximately 30% based on N transformation pathways reported for high-rate pond systems [25]. Of this denitrified fraction, 99% was assumed to be converted to nitrogen gas (N_2) and 1% to N_2O [28], [26]. Additional non-assimilatory N removal was assigned to particulate or inert accumulation and sedimentation (15%), representing retained non-gaseous N associated with solids retention [25]. NH_3 volatilization was assigned 2%, using the low end of reported literature values because NH_3 was not detected in the laboratory system after 1–3 days (Appendix Figure A12) [25], [38]. A similar approach was used to complete the phosphorus balance, with results presented in Appendix Section A7 and Figure A16 [39], [40], [41], [42], [43].

2.3.2 Biokinetic Parameter Estimation

After average nutrient removal rates were determined, Monod kinetic parameters were estimated to represent concentration-dependent N and P uptake. These parameters included the half-saturation constant (K_s), defined as the substrate concentration at which uptake reaches half of its maximum rate, and the maximum substrate uptake rate (r_{max}), which represents uptake under non-limiting substrate availability. Unlike the average removal rates (R_s) calculated from section 2.3.1, r_{max} represents the expected removal rate under optimal substrate availability. Daily concentration data were used to construct substrate depletion curves and fit the Monod model (Appendix Section A8). Controlled-system assumptions were applied because microorganisms such as cyanobacteria can compete for nutrients and affect algal growth [44], [45]. Therefore, pH and operating conditions were assumed to minimize community shifts, nutrient competition, and productivity inhibition. Biomass decay was neglected because its contribution was expected to be minor and insufficient data were available for reliable estimation [36], [46], [47].

The final Monod-derived model was expressed as:

$$t_2 - t_1 = \frac{V}{A * r_{max}^{(A)}} \left[(S_1 - S_2) + K_s \ln\left(\frac{S_1}{S_2}\right) \right] \ [\boldsymbol{Eq.3}]$$

Where t_1 and t_2 are the initial and subsequent sampling times (day), V is the water system volume (L), A is the effective ATS surface area (m^2), $r_{\max}^{(A)}$ is the areal maximum substrate utilization rate (mg substrate m^{-2} day^{-1}), S_1 and S_2 are the substrate concentrations at $t_1$and t_2 (mg L^{-1}), and K_s is the half-saturation constant (mg L^{-1}).

The kinetic parameters K_s and $r_{max}^{(A)}$ were estimated by fitting the model to the experimental data using sum of squared errors (SSE) minimization [48]. After a two-week acclimation period under high-nutrient conditions, daily nutrient-concentration data were collected for 24 days from the stabilized ATS biofilm. Fitting was performed separately for each harvest period using Eq. 3, allowing kinetic parameters to be estimated from the initial and final nutrient concentrations of each cultivation period. For each observation, the model-predicted time interval was compared with the observed experimental interval, and final kinetic parameters were reported as the average of the harvest-specific estimates.

2.3.3 Coupled Hydraulic–Biokinetic Process Model

After the kinetic parameters were estimated, hydraulic recirculation was coupled with Monod-based nutrient uptake to simulate the cultivation process (Appendix Section A9). Nutrient removal during each pass over the algal surface was limited by the Monod uptake capacity and constrained by recirculation rate, ATS surface area, and time between harvests [36]. The sizing function therefore estimated the ATS cultivation area (A_{ATS}) and the number of recirculation days required to meet target effluent concentrations. A maximum treatment period of seven days was imposed as an operational constraint based on pilot-scale systems operated by HydroMentia [49], after which biomass decay becomes non-negligible.

The biokinetic framework used a recirculating tank–ATS configuration with constant water volume and negligible evaporation losses. The recirculation water tank concentration was assumed to represent the ATS influent concentration. Because the algal community was periphytic, biomass accumulation in the water column was neglected, and nutrient removal was modeled as surface-attached algal uptake [50], [51]. At each time step, water flowed from the tank through the ATS channels, where N and P were removed according to flow rate, cultivation area, productivity, biomass composition, and Monod-based uptake kinetics, before returning to the tank and updating the mixed concentration during recirculation.

Hence, the coupled tank-ATS derivation resulted in the following two equations:

$$Q_w(S_n - S_{out,ATS}) = A_{ATS} * J_{max} \frac{S_{out,ATS}}{K_s + S_{out,ATS}} \ [\boldsymbol{Eq. 4}]$$

$$S_{n+1} = (S_n - S_{out,ATS})e^{-k_w \Delta t} + S_{out,ATS} \ [\boldsymbol{Eq. 5}]$$

Where Q_w is the water flow rate (L day^{-1}), S_n is the water tank concentration at the beginning of each time step and the ATS inlet concentration (mg L^{-1}), $S_{out,ATS}$ is the ATS outlet concentration returning to the tank (mg L^{-1}), A_{ATS} is the cultivation area being evaluated (m^2), J_{max} is the maximum substrate uptake flux based on productivity and biomass nutrient composition (mg substrate m^{-2} day^{-1}), K_s is the half-saturation constant (mg L^{-1}), S_{n+1} is the updated water tank concentration after the time step (mg L^{-1}), k_w is the tank recirculation rate (day^{-1}), and Δt is the numerical time step used to update the tank concentration (day).

The known model inputs included $K_s, J_{max}, Q_w, V_T, k_w$, initial concentration, and effluent target concentration. The K_s values calculated from the laboratory biokinetic model were retained in the sizing model to define concentration-dependent uptake; however, the experimental $r_{max}^{(A)}$ was not applied directly. Instead, the maximum uptake term was expressed as J_{max}, reflecting the maximum uptake capacity is supported by light-driven biomass productivity and biomass nutrient composition in an established ATS turf. This assumption may differ during start-up, when turf establishment and biomass accumulation can limit nutrient uptake. ATS area and recirculation time were evaluated iteratively as design variables. At each time step, the model solved the ATS outlet and updated tank concentrations, then compared the tank concentration with the effluent target to determine whether the area-time combination met the treatment requirement within the seven-day limit.

2.4 Design constraints and system sizing

2.4.1 Lagoon influent assumptions and ATS model design constraints

Proper hydraulic design is critical for lagoon performance. The lagoon was assumed to operate under optimal conditions based on Pfost et al. [52] and Schmidt et al. [53], including centrally located or distributed inlets, operation at one-third to one-half capacity, continuous flushing-system loading, and periodic agitation during pump-down and sludge removal to reduce solids accumulation, odors, and treatment limitations. Because anaerobic lagoons typically have long hydraulic residence times, short-term ATS recirculation was not expected to create hydraulic constraints or water accumulation that would compromise lagoon performance [10].

ATS sizing was constrained by hydraulic guidelines from HydroMentia and Ryland et al. [19], including a linear hydraulic flow-rate (LHFR) of 2.1-8.3 L s^{-1} m^{-1} and a channel length-to-width ratio (L:W) of 2:4 [13], [19]. Each ATS module was assumed to have a minimum constructable area of 1 acre, while the maximum allowable area was scaled from the HydroMentia baseline of 2.5 acres per 10 MGD of wastewater flow [54]. Although smaller systems may be technically feasible, systems below 1 acre were excluded from the design space because construction, infrastructure, and operational costs were considered economically impractical [19].

2.4.2 System Sizing

The ATS system was sized using productivity and hydraulic constraints summarized in Table 1. For a given influent flow, longer recirculation times allow nutrient uptake to accumulate over multiple days, reducing the cultivation area required to meet effluent targets. The model iteratively tested treatment area and recirculation time to identify the smallest feasible ATS configuration capable of meeting N and P limits. To support practical implementation, the required area was divided into modular grid-based layouts (Appendix Figure A10), avoiding irregular channel layouts and allowing module replication. As a conservative design buffer, effluent targets were set to 20% less of the nutrient target limit to reduce the risk of exceedance under uncertainty in productivity, nutrient-removal kinetics, and county-level scaling. The final cultivation model selected the configuration with the lowest minimum biomass selling price (MBSP) while satisfying hydraulic constraints and effluent targets.

Table 1. Summary of cultivation model parameters, biomass composition assumptions, and ATS operational/design variables used for spatial simulations

Parameter	Value	Units	Reference
Cultivation Model			
Target Total Nitrogen	2.14 – 30.64 (Grass-min Scenario)	mg L^{-1}	[30], [37]

Target Total Phosphorus	0.45 – 6.42 (Grass-min Scenario)	mg L^{-1}	[30], [37]
Inlet Total Nitrogen	730 (Diluted to 100)	mg L^{-1}	[22], [34], [9]
Inlet Total Phosphorus	160 (Diluted to 22)	mg L^{-1}	[22], [34], [9]
Flow Rate	County-resolved (varied)	MGD	[22], [34], [9]
Operational Days	County-resolved (varied)	days	[20]
Global Horizontal Irradiation (GHI)	County-resolved (varied)	W m^{-2}	[20]
Light Efficiency	2.71	%	Experimentally Validated
Biomass Elemental Composition			
Ash	20	% of solids	Experimentally Validated [19]
Carbon	50	% of ash free solids	Experimentally Validated [19]
Nitrogen	10	% of ash free solids	Experimentally Validated [19]

Phosphorus	1	% of ash free solids	Experimentally Validated [19]
Nitrogen to Phosphorus Molar Ratio	22	Ratio	Experimentally Validated [19]
Algal Turf Scrubber Design Variables			
Linear Hydraulic Flowrate	2.07 – 8.28	L s^{-1} m^{-1}	[13], [19]
Length to Width Ratio	2 – 4	Ratio	[13], [19]
Pump Energy Use	0.096	kWh m^{-3}	[13], [19]
Other Energy Use	10	% of pump energy	[13], [19]
Area per module	1 – 2.5	acres	[54]
Maximum recirculation time	7	days	[49]

2.5 HTL conversion model

The modeled pathway for converting algae into renewable diesel began with wet-harvested biomass mechanically concentrated by centrifugation to approximately 20 wt% solids [21]. Under high-temperature and high-pressure HTL conditions, algal biopolymers, including proteins, carbohydrates, and lipids, were converted into biocrude, aqueous products, gases, and residual solids [56]. The HTL model was based on Chen et al. [21], with ash-reduction methods from Banks et al. [20]. Biocrude was upgraded into diesel, naphtha, and heavy oil fractions, with the heavy oil further hydrocracked to increase diesel and naphtha yields. For each state, the HTL facility was assumed to be centralized in the county with the highest dairy cattle inventory, and harvested algae from all other counties in that state were transported to this facility.

The HTL aqueous product was assumed to be sold as a fertilizer product due to its recoverable nitrogen and phosphorus content, while HTL solids were treated as a biochar co-product with the potential for carbon sequestration. Feedstock solids were assumed to contain 5.2% lipids, 51.6% proteins and 31% carbohydrates, based on DeRose et al. [55]. Additional HTL parameters are summarized in Ryland et al. [19]. Because raw biocrude contains heteroatoms, particularly nitrogen, oxygen, and sulfur, upgrading was required before use as a transportation fuel blendstock. Upgrading was modeled through hydrotreating to stabilize the oil and remove heteroatoms via hydrogenation, denitrogenation, desulfurization, and deoxygenation reactions [21], [56].

2.6 Techno-Economic Assessment

2.6.1 TEA Framework and Cost Assumptions

The TEA included capital expenditures (CAPEX), operating expenses (OPEX), revenue generation, 7-year depreciation using the IRS MACRS schedule for biofuel production, and a 10% internal rate of return (IRR) [57]. CAPEX included both direct and indirect costs to estimate fixed capital investment (FCI), while OPEX included fixed and variable operating costs. All results were reported in 2024 U.S. dollars by indexing equipment costs with the Chemical Engineering Plant Cost Index [58], chemical costs with the Producer Price Index by Commodity [59], and labor costs with Current Employment Statistics[60]. A discounted cash flow rate of return (DCFROR) analysis was used to calculate the minimum biomass selling price (MBSP) and minimum fuel selling price (MFSP) at a net present value of zero and 10% IRR. Financial parameters followed “Nth-of-a-kind plant” assumptions from the U.S. Department of Energy, as summarized by Ryland et al. [19], [61].

ATS facility costs were based on HydroMentia data and used for the conservative cost case [13]. The optimistic cost case used updated assumptions from DeRose et al. [62], and all costs were scaled to 2024 using CEPCI [58]. These two cases were included to bracket uncertainty in large-scale ATS deployment costs, with the conservative case representing commercial capital costs and the optimistic case reflecting lower-cost attached-algal-system estimates. Land costs were estimated from county-level USDA marginal land prices suitable for non-food, non-residential development [63]. Recirculation tank costs were based on required storage volume and scaled using EPA tank cost curves [64]. State-level industrial electricity prices from the 2024 costs U.S. Energy Information Administration (EIA) Electric Power Monthly dataset were used to capture geographic variability in power costs [65]. Downstream processing costs, HTL co-product credits, and economic assumptions followed Ryland et al. [19] and were indexed to 2024 USD.

2.6.2 Scenario Analysis

Scenario analyses were used to evaluate ATS economic feasibility under different costs, product values, and credit assumptions. MBSP and minimum wastewater selling price (MWSP) were first calculated under conservative and optimistic cost scenarios. The resulting MBSP values were then used as biomass feedstock costs in the downstream HTL model to calculate MFSP. A nutrient-credit scenario was used to estimate the N and P credit values ($ kgN^{-1} and $ kgP^{-1}) required to reach the target fuel selling price of $0.98 LGE^{-1} (liter gasoline equivalent), equivalent to $3.71 GGE^{-1} (gallon gasoline equivalent). Finally, sensitivity and uncertainty analyses identified the most influential input parameters and estimated ranges for MBSP, MWSP, and MFSP under parameter variability.

2.6.3 Nutrient Credit Lookup Function

Nutrient credits were incorporated into the TEA to estimate the compensation required for ATS-based N and P removal to become economically viable. Nutrient pollution remains a persistent water-quality challenge [66], and dairy effluent management has increasingly been associated with regulatory attention and enforcement related to nutrient losses [67], [68], [69]. As water-quality pressures increase, ATS systems may provide a practical, lower-operating-cost option for nutrient removal. Previous studies have evaluated dairy wastewater co-treatment in municipal wastewater treatment plants (WWTPs) [19], but these pathways rely on centralized infrastructure and may not be applicable to dispersed dairy lagoon systems [70].

To compare ATS nutrient-removal economics with existing treatment benchmarks, this study used the nutrient credit framework from Limb et al. [71], which relates N and P removal values to wastewater treatment levels. However, the absolute values from that framework were not applied directly because they represent municipal wastewater treatment conditions rather than decentralized dairy lagoon treatment. Instead, nutrient credits were estimated using a reverse-pricing approach. The model first calculated the total credit value required for the ATS-to-renewable-diesel pathway to reach a target fuel selling price of \$0.98 LGE^{-1} (\$3.71 GGE^{-1}), which was selected based on average U.S. fuel prices [72]. This total value was then distributed between N and P credits using the relative N:P credit structure from Limb et al. [71] and the effluent targets defined for each crop-based reuse scenario [30].

This approach preserved the relative N:P structure of the framework presented in Limb et al. [71] while adapting credit values to the treatment goals and economics of this study (Appendix Section A10). The resulting N and P credit requirements were compared with current nutrient-removal cost benchmarks to evaluate whether ATS-based nutrient recovery could be competitive with existing treatment technologies.

2.7 Life Cycle Assessment

An attributional LCA was used to assess the environmental impacts of renewable diesel produced through the modular ATS system. The well-to-wheels boundary included biomass cultivation, HTL fuel production, and end-use combustion. Infrastructure and initial water inputs were excluded because their contributions were considered negligible over the 30-year project lifetime. Transportation emissions were included by assuming that harvested algae from each county were transported to a centralized HTL facility located in the county with the highest dairy cattle inventory within each state. The functional unit was the production and use of 1 MJ of total fuel, including both naphtha and renewable diesel.

Co-product credits were assigned to recovered nutrients from the HTL aqueous phase and carbon storage in HTL solids. Recovered N and P were credited as avoided conventional fertilizer production, displacing the upstream energy use, material inputs, and emissions associated with synthetic nutrient production. Life cycle inventory (LCI) data were sourced from ecoinvent version 3.11 [73], TRACI 2.1 was used for impact assessment following Chen et al. [21], with N_2O emissions and NH_3 volatilization from the cultivation model added to represent the high-nutrient characteristics of anaerobic lagoon effluent. Ten impact categories were evaluated, including global warming potential (GWP), eutrophication, acidification, ecotoxicity, ozone depletion, photochemical ozone formation, fossil fuel depletion, particulate matter, and carcinogenic and non-carcinogenic human health effects [74]. For 100-year GWP, characterization factors of 1, 29.8, and 273 were used for CO_2, CH_4, and N_2O, respectively, based on the IPCC Sixth Assessment Report [38].

For the GWP breakdown, a minus-one/plus-one analysis was applied to track biogenic carbon across the ATS-to-fuel pathway. Carbon uptake during algal growth was assigned as CO_2 uptake credit, while biogenic carbon released during HTL processing, upgrading, and end-use fuel combustion were counted as process burdens. Additional fossil and process emissions from cultivation, harvesting, transportation, HTL processing, and upgrading were included as emissions burdens. This approach fully quantified algal carbon uptake, downstream carbon release, process emissions, and co-product credits within the integrated wastewater treatment and renewable fuel pathway.

2.8 Sensitivity and Uncertainty

Two uncertainty-evaluation approaches were used. A fixed-percentage single-factor sensitivity analysis identified the input variables with the greatest influence on system performance, while a Monte Carlo analysis quantified the combined effect of parameter uncertainty on cultivation and HTL model outputs.

2.8.1 Sensitivity Analysis

Sensitivity analysis was conducted to identify the input parameters with the greatest influence on cultivation performance, fuel production economics, wastewater treatment economics, and environmental outcomes. Each parameter was varied independently by ± 20% from its baseline value while all other parameters were held constant. This one-at-a-time approach identified the assumptions that most strongly affected model outputs.

For the cultivation model, sensitivity parameters included algal productivity, light-use efficiency, nutrient uptake kinetics, ATS capital costs, operational costs, and energy requirements. Weld County, Colorado, was selected as the representative location because it provided an intermediate case between highly favorable and less favorable deployment scenarios identified in the national assessment. Compared with California counties, which combine high algal productivity with large dairy inventories, and Wisconsin counties, which have substantial dairy populations but lower productivity, Weld County exhibits moderate productivity while maintaining a significant dairy inventory of 134,728 dairy cattle. In addition, approximately 30% of dairy manure in Colorado is managed through anaerobic lagoons, making Weld County representative of locations where ATS deployment could be integrated with existing lagoon-based manure-management infrastructure.

For the HTL pathway, sensitivity parameters included biomass feedstock cost, algae composition, capital costs, operating costs, and co-product credits for the centralized Colorado biorefinery. The outputs evaluated were MBSP, MFSP, MWSP, and GWP. Results are presented as tornado plots in SI Section A5, where larger bars indicate greater parameter influence on model outcomes.

2.8.2 Monte Carlo Analysis

Monte Carlo analysis was performed in two stages to quantify uncertainty in both the cultivation and HTL model outputs. For the cultivation model, the five most influential parameters identified from the sensitivity analysis were varied: light-use efficiency, N half-saturation constant (K_s,N), N uptake rate, cultivation system cost, and algal solids content. Parameter uncertainty was defined using baseline values, literature-informed standard deviations, and bounded distributions to avoid unrealistic samples [24], [75], [76], [77], [78], [79]. Detailed baseline values, standard deviations, bounds, and sampling assumptions are provided in Appendix Section A11.

For the HTL model, uncertainty was quantified considering variations in biomass selling price, total wet algae feedstock, and biomass composition for the Colorado HTL model. Biomass selling price and feedstock distributions were obtained from the cultivation Monte Carlo results, while protein, carbohydrate, and lipid fractions were varied using literature-informed triangular distributions based on Valdez et al. [56], Wang et al. [80], and Gong et al. [81]. Detailed HTL input distributions and scaling assumptions are provided in Appendix Section A11.

Monte Carlo convergence was evaluated using 1,000, 5,000, and 10,000 simulations. The distributions from 5,000 and 10,000 simulations showed no meaningful differences in central tendency, spread, or overall shape; therefore, 5,000 simulations were used for the final uncertainty analysis to balance stability and computational efficiency. Results are reported using the central 90% confidence interval, defined by the 5th and 95th percentiles.

To reduce computational time, cultivation uncertainty was propagated to the HTL model using relative scaling rather than rerunning Monte Carlo simulations for every county. For each state-level biorefinery, the representative county was used to obtain the mean and standard deviation of biomass selling price and total algae feedstock from the cultivation Monte Carlo analysis. These values were normalized by the corresponding baseline values to generate dimensionless scaling factors, which were then applied to the baseline biomass cost and feedstock inputs of the state-level HTL facility. This approach preserved regional consistency while reducing computational demand.

3. RESULTS AND DISCUSSION

Experimental parameterization and TEA/LCA results are presented for ATS-based nutrient remediation and renewable diesel production scenarios. Results include experimental/model parameterization (Section 3.1), regional ATS performance and system sizing (Section 3.2), Nutrient-credit scenarios (Section 3.3), LCA results (Section 3.4), sensitivity and uncertainty analysis (Section 3.5), and deployment implications (Section 3.6) and model limitations (Section 3.7).

3.1 Experimental/Model Parameterization

3.1.1 Nutrient Uptake

Experimental TN and TP removal rates for the 100 ppm-N, 10:1 N:P flow-way are summarized in Table 2. These results distinguish total removal ($R_{s,total}$), biomass-associated uptake ($R_{s,biomass}$), and the remaining removal assigned to additional removal pathways ($R_{s,others}$). This breakdown shows that nutrient removal was not controlled only by algal biomass assimilation, but also by secondary removal mechanisms.

Table 2. Nitrogen and phosphorus removal rates in the ATS system operated at 100 ppm-N and a 10:1 N:P ratio. Total removal rates were separated into biomass-associated uptake and other removal pathways. Values are reported as mean ± standard deviation.

Parameter	Nitrogen ($g\ N\ m^{-2}\ day^{-1}$)	Phosphorus ($g\ P\ m^{-2}\ day^{-1}$)
$R_{s,total}$	4.35 ± 1.12	0.43 ± 0.18
$R_{s,biomass}$	1.82 ± 0.42	0.18 ± 0.04

$R_{s,others}$	2.53 ± 1.14	0.25 ± 0.18

The 100 ppm-N flow-way results indicate that approximately 42% of TN and TP removal is associated with algal biomass and slough, while the remaining 58% is attributed to additional removal pathways. Biomass-associated uptake rates are comparable to high-nutrient algal treatment values reported by Mulbry et al. [24], including 1.58 ± 0.14 g N m^{-2} day^{-1} and 0.22 ± 0.02 g P m^{-2} day^{-1} [24]. The observed 42/58 distribution in Table 2 is also consistent with the 40–60% biomass-assimilation range reported in previous high-nutrient algal treatment studies [12], [24]. The pathway distribution is provided in Appendix Figure A16.

In the cultivation model, 42% of the TN and TP removal is represented by biomass-associated uptake, calculated from light-use-efficiency-based biomass productivity and assumed biomass composition. The remaining 58% are assigned to non-biomass removal pathways. Thus, total nutrient removal is modeled as the combination of algal biomass uptake and additional removal mechanisms.

3.1.2 Bio-Kinetic Monod Model Parameters

Monod kinetic parameters were estimated by fitting Eq. 3 to the experimental concentration data using SSE minimization. The resulting average half-saturation constants ($K_{s,avg}$) and maximum nutrient uptake rates ($r_{max,avg}$) are summarized in Table 3. These parameters are used to represent concentration-dependent nutrient removal in the coupled hydraulic-biokinetic model.

Table 3. Biokinetic parameters estimated for nitrogen and phosphorus uptake in the ATS system. Values include the average half-saturation constants ($K_{s,avg}$) and maximum nutrient uptake rates

(r_{max}) separated into total average uptake, biomass-associated uptake, and other removal pathways. Values are reported as mean ± standard deviation where applicable.

Parameter	**Nitrogen**	**Unit**	**Phosphorus**	**Unit**
$K_{s,avg}$	13.49 ± 5.17	mgN L^{-1}	1.45 ± 1.10	mgP L^{-1}
$r_{max,avg}^{(A)}$	9.76 ± 3.17	gN m^{-2} day^{-1}	0.45 ± 0.08	gP m^{-2} day^{-1}

Direct comparison of $K_{s,avg}$ values with other ATS systems is limited because ATS communities are mixed assemblages of algae, bacteria, and other microorganisms, and species-specific kinetic parameters are rarely reported. Therefore, the estimated $K_{s,avg}$ values in Table 3 are compared with controlled studies of freshwater microalgae. For N, the estimated $K_{s,avg}$ is comparable to values of 11.8 and 12.1 mg N L^{-1} reported for *Scenedesmus* sp. [75], [76], and 14.23 ± 2.17 mg N L^{-1} reported for *Chlorella protothecoides* [77]. For P, the estimated $K_{s,avg}$ is higher than the 0.27-0.28 mg P L^{-1} reported for *Scenedesmus* sp. [75], [76], but comparable to the 1.8 ± 0.28 mg P L^{-1} reported for *Chlorella protothecoides* [77]. These comparisons do not imply similar species composition but indicate that the fitted kinetic parameters are consistent with reported freshwater algal nutrient uptake behavior.

The estimated r_{max} values are higher than the average removal rates reported in Table 2, which is expected because average rates reflect weekly observed removal under varying conditions, whereas r_{max} represents the maximum substrate utilization rate predicted by the Monod model. This relationship supports the internal consistency of the fitted parameters. For P, r_{max} values are closer to the observed removal rates than for N, suggesting that P availability is a stronger constraint on uptake during cultivation. This is consistent with the experimental N:P ratio, where N concentrations are approximately one order of magnitude higher than P concentrations. Model-estimated nutrient concentrations were compared with experimental observations to evaluate goodness of fit (Appendix Figure A13). The model shows strong agreement for both nutrients, with R^2 values of 0.9447 for N and 0.9874 for P. These results support the reliability of the fitted kinetic parameters and their use in the coupled hydraulic-biokinetic model.

3.2 Regional ATS performance and system sizing

Cultivation and HTL results indicate that ATS-derived algae are not economically viable for renewable diesel production under either cost scenario without nutrient credits. Spatially resolved results in Figure 2 show substantial MBSP, MWSP, MFSP variability across the United States. For biomass generation, all counties exceed the baseline algae cost of \$0.47 kg^{-1} reported by the International Energy Agency (IEA) Bioenergy [82], under conservative costs (Figure 2A), with MBSP values ranging from 1.61–9.70 \$ kg^{-1}. Under optimistic cost assumptions (Figure 2B), MBSP decreases substantially to 0.20–4.00 \$ kg^{-1}, with 86% of counties falling below the IEA baseline, reflecting the strong influence of reduced cultivation costs and improved system performance. These results indicate that lower ATS capital and operating costs can substantially improve biomass economics, but biomass production alone remains insufficient to make the downstream renewable diesel pathway competitive without nutrient-removal value.

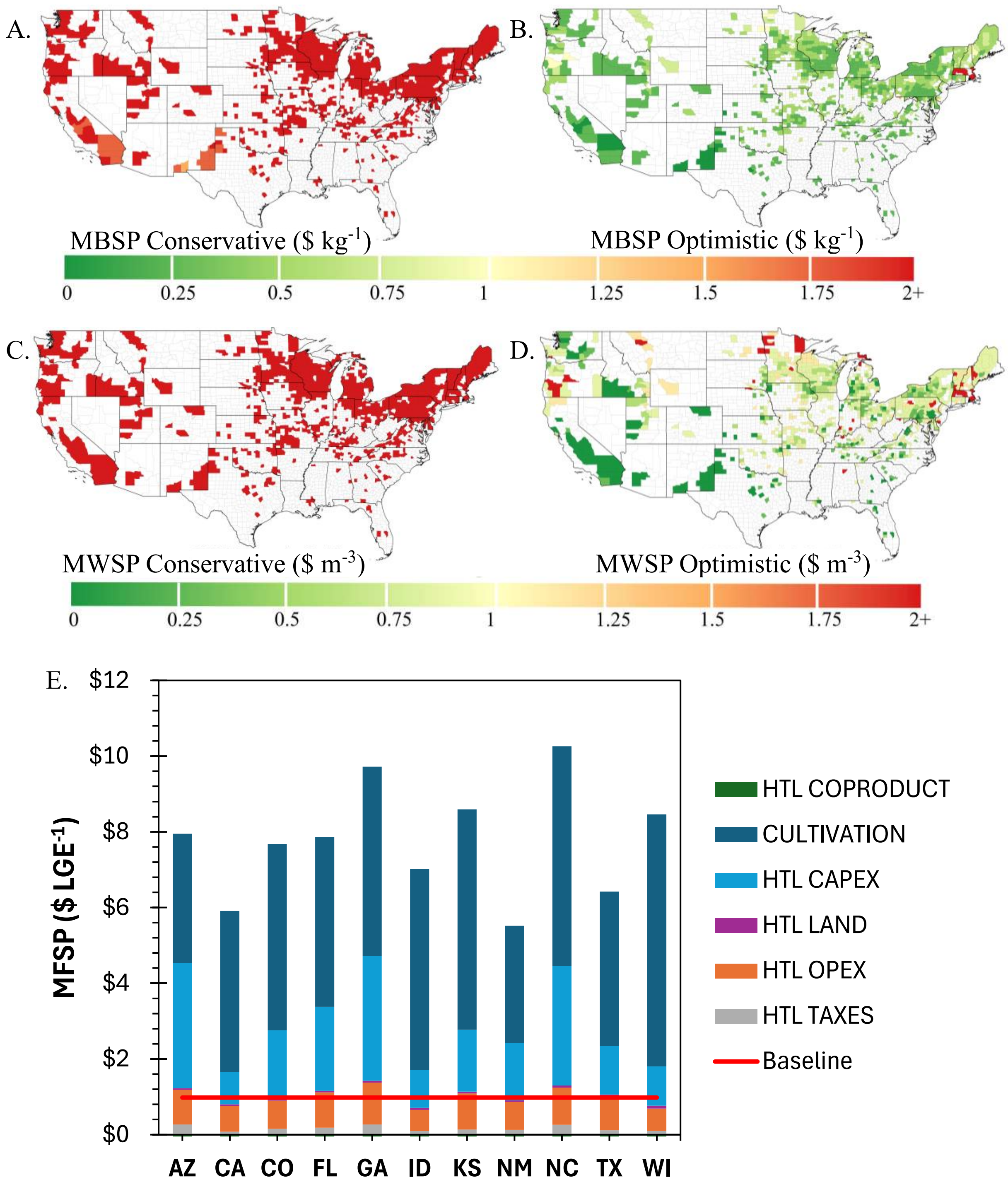

Figure 2. Spatial distribution of ATS economic outcomes across the contiguous United States (CONUS) and MFSP breakdown for representative biorefineries. Panels A–D present spatial outcomes under conservative cost assumptions in the left column and optimistic cost assumptions in the right column. Panels A–B show the minimum biomass selling price (MBSP, $ kg^{-1} algae)

relative to a \$0.47 kg^{-1} biomass benchmark, while panels C–D show the minimum wastewater selling price (MWSP, \$ m^{-3}). Panel E shows the MFSP breakdown for 10 representative biorefineries under the optimistic nutrient-credit scenario required to meet the baseline \$0.98 LGE^{-1} target fuel price. Cost components include ATS cultivation, HTL CAPEX and OPEX, land cost, and taxes; negative values represent coproduct credits from biochar, displacement of conventional fertilizers including diammonium phosphate (DAP) and ammonia (NH_3), as well as N and P removal credits. White areas in the maps indicate missing data, no qualifying anaerobic lagoon systems, locations where lagoons were not required under EPA criteria, or sites with no feasible ATS configuration.

Regional MBSP and MFSP patterns are primarily influenced by lagoon flow availability, operational days, solar irradiance, and algal composition. Lower MBSP values generally occur in the southwestern U.S., where favorable irradiance and longer operating periods support greater algal productivity and distribute cultivation costs across higher annual biomass production. Some southeastern states also show promising performance because adequate solar availability and extended operating windows offset moderate productivity (Appendix Figure A5). In contrast, many Midwestern states are less favorable because lower solar irradiance and shorter operating seasons limit algal growth despite high manure availability and lagoon flow. Operational days range from 340–365 days in parts of the northwestern U.S., compared with 220–240 days in portions of the Midwest. These patterns highlight that climate-driven operating periods, together with flow availability and productivity, shape regional ATS economic performance.

Spatial variability in ATS performance is also strongly affected by the effluent flow, which depends on county-level manure production and the fraction of manure managed in anaerobic lagoons (Appendix Figure A15). Vermont and Massachusetts provide a clear example: both have counties with similar dairy cow inventories, but Vermont sends approximately 27% of manure to lagoons, whereas Massachusetts sends only about 1%, with most manure managed in deep pits, on pasture, or in other systems [35]. As a result, similar herd sizes do not necessarily produce similar lagoon flow or ATS potential. This relationship between effluent flow and regional operating conditions also explains why states with moderate-to-high lagoon use and favorable climates show stronger ATS potential. California, for example, directs about 24% of manure to lagoons [35], and its favorable climate supports higher algal productivity. In contrast, Wisconsin has high dairy density and substantial lagoon loading, but lower solar irradiance limits productivity and increases both MBSP and MFSP. Overall, ATS economic performance depends on the balance among lagoon flow, algal productivity, annual operating days, cultivation costs, and biorefinery logistics.

For wastewater treatment, all conservative cost assumptions values exceed the \$1.61 m^{-3} MBR + side-stream RO benchmark, as shown in Figure 2C, with MWSP values ranging from 3.89–30.43 \$ m^{-3}. Under optimistic cost assumptions (Figure 2D), MWSP decreases to 0.49–3.80 \$ m^{-3}, with 94% of evaluated ATS systems falling below this benchmark without applying nutrient credits. Although the optimistic case lowers MWSP across all evaluated locations, regional trends remain similar between scenarios: lower MWSP values generally occur in regions with greater lagoon flow availability, longer operating periods, and favorable irradiance, while higher values occur where limited qualifying lagoon flow or shorter operating seasons reduce annual treatment capacity relative to installed ATS infrastructure. he contrast between the conservative and optimistic cases shows that ATS treatment competitiveness is strongly driven by modular ATS and peripheral infrastructure costs, consistent with the lower ATS cost assumptions derived from DeRose et al. [62]. Overall, lagoon-based ATS systems appear valuable as a nutrient-recovery technology, particularly when their treatment benefits are compared with conventional nutrient-removal pathways.

For renewable diesel production, MFSP values remain above the target fuel selling price of \$0.98 LGE^{-1} (\$3.71 GGE^{-1}) [72] even under optimistic costs as shown in figure 2E. Conservative-cost MFSP ranges from \$26.42-79.26 LGE^{-1} (\$100-300 GGE^{-1}) while optimistic-cost MFSP decreases to \$5.45-23.78 LGE^{-1} (\$20.6-90 GGE^{-1}). Spatially resolved MFSP results for all evaluated states are provided in Appendix Figure A7. The cost breakdown in Figure 2E indicates that ATS cultivation costs remains the largest contributor to MFSP, with HTL CAPEX also representing an important cost component. Therefore, improvements in ATS cultivation costs and HTL capital efficiency are critical for reducing renewable diesel production costs toward competitive fuel prices without relying solely on nutrient-removal credits. However, because the system is also designed for nutrient recovery, nutrient credits remain an important mechanism for recognizing the treatment value provided by lagoon-based ATS deployment, consistent with Ryland et al. [19], who found that wastewater flow and nutrient-removal value are critical drivers of ATS economic performance. This supports the interpretation that ATS-to-HTL systems are most viable when fuel production is coupled with nutrient-recovery credits.

After evaluating unit production costs, total renewable fuel output was assessed to determine whether ATS-derived renewable diesel could contribute meaningfully to national fuel demand if the pathway became economically viable. California exhibits the highest renewable fuel production, reaching 3.96 million liters of gasoline equivalent (MMLGE) per year (1.05 MMGGE yr^{-1}) (Appendix Figure A9). This represented approximately 19% of the total 20.67 MMLGE yr^{-1} (5.46 MMGGE yr^{-1}) produced across all evaluated states. However, total modeled fuel production remained small compared with current U.S. gasoline demand, estimated at 517,485 MMLGE yr^{-1}

(136,720 MMGGE yr^{-1}) in 2025 [83]. Together, these results show that ATS-derived renewable diesel is limited by both high production costs and insufficient fuel output to meaningfully offset national fuel demand.

3.3 Nutrient -credit scenarios

Nutrient credits substantially improve the economic outlook of the ATS-to-HTL pathway. Under conservative assumptions, as shown in Figure 3, approximately 30% of locations require N credits below conventional N treatment costs of \$42 kg N^{-1} (Figure 3A), while 65% require P credits below conventional P treatment costs of \$321 kgP^{-1} (Figure 3B). Under optimistic assumptions, this increases to 96% of locations for both nutrients, with only a few low-flow cases, such as Massachusetts and Wyoming, remaining above these benchmarks. Because lagoon effluent contains substantially more N than P, N removal represents a larger recoverable nutrient mass; however, conventional N treatment costs are lower on a per-kg basis, so fewer locations fall below the N benchmark under conservative assumptions. In contrast, P has lower mass loading in the effluent, but higher conventional P treatment costs make ATS-based P recovery more competitive relative to the benchmark, leading to a larger share of locations below the P benchmark. These results indicate that ATS-derived renewable diesel becomes economically more competitive when the nutrient-removal service is valued, and that in many locations the required N and P credits are lower than conventional treatment costs. Therefore, the ATS-to-HTL pathway is most viable not as a stand-alone fuel-production system, but as an integrated water-treatment technology that can co-produce renewable fuel while providing treatment services at competitive or lower costs.

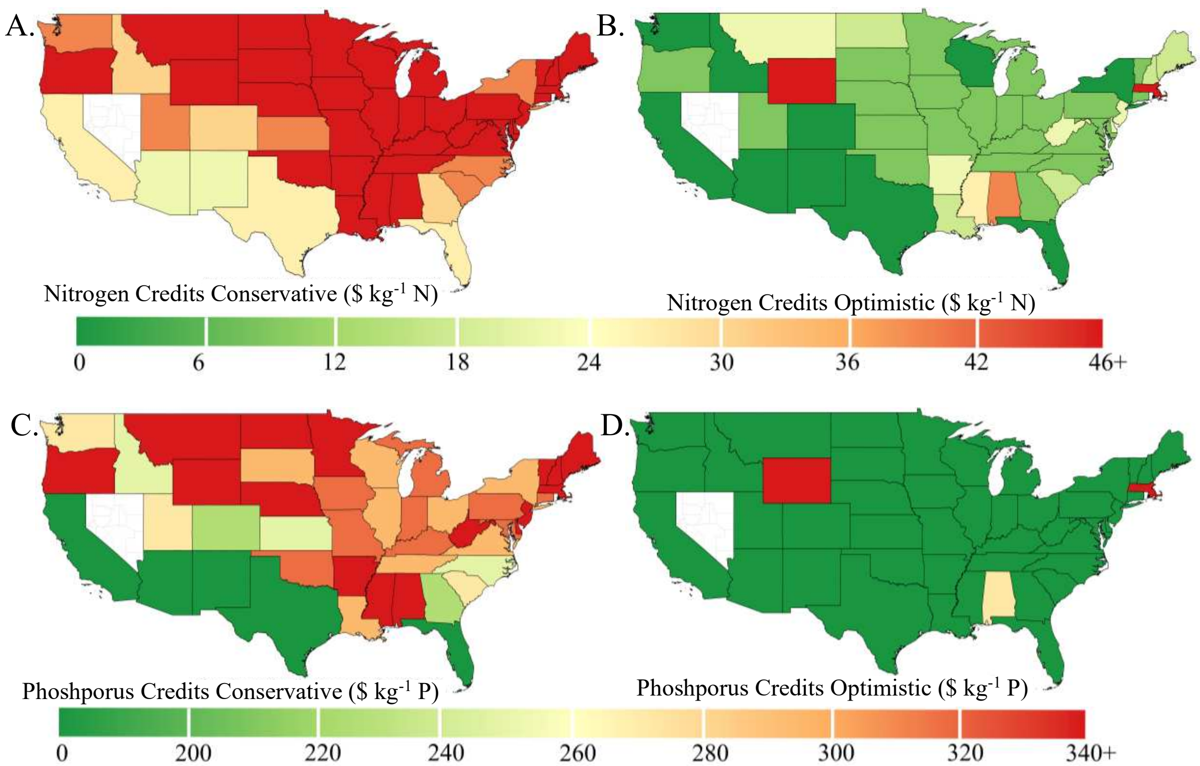

Figure 3. Spatial distribution of nutrient credits required to reach the target MFSP across the contiguous United States (CONUS), with conservative cost assumptions shown in the left column and optimistic cost assumptions shown in the right column. Panels A–B show required nitrogen credits ($ kg^{-1} N) relative to the conventional N treatment benchmark of $42 kg^{-1} N, while panels C–D show required phosphorus credits ($ kg^{-1} P) relative to the conventional P treatment benchmark of $321 kg^{-1} P. Green areas indicate locations where required credits are below the corresponding treatment benchmark, while warmer colors represent progressively higher credit requirements. White areas indicate missing data, zero wastewater flow, or sites excluded from the analysis.

These findings indicate that nutrient credits are required to reach the target MFSP, but the required credit levels remain below conventional N and P treatment costs in many locations. Locations with higher algal productivity, longer operating periods, higher solar irradiance, and sufficient lagoon flow, including California and New Mexico in the Southwest as well as Florida and Georgia in the Southeast, require lower credits to achieve competitive fuel production costs, as reflected by the regional patterns in Figure 3. These states are potential early adopters of ATS-to-HTL deployment because they can combine renewable fuel production with nutrient-removal services at credit levels below conventional treatment benchmarks. Therefore, ATS-to-HTL feasibility depends not only on fuel conversion performance, but also on site-specific productivity and lagoon flow availability, which determine the nutrient-credit levels required to reach competitive fuel costs.

3.4 Life Cycle Assessment

Net GHG emissions were evaluated for the full ATS-to-HTL fuel pathway to assess geographic variation across the United States. Full-pathway GWP results are discussed in Section 3.4.1 and compared with the Renewable Fuel Standard (RFS) threshold of 45 g CO_2e MJ^{-1} to provide regulatory context [84]. Representative state-level GWP breakdowns are evaluated in Section 3.4.2 to identify the contribution of cultivation, CO_2 uptake, HTL processing, upgrading, transport, and combustion to net emissions. Additional TRACI impact categories are analyzed in Section 3.4.3.

3.4.1 Life Cycle Assessment Results

GWP results across CONUS are presented in Figure 4 and compared with the RFS threshold. Most evaluated locations range from 60 to 200 g CO_{2e} MJ^{-1}, exceeding the threshold by a factor of 2-4 when the ATS-to-fuel pathway is considered, including cultivation, harvesting, biomass transport, HTL processing, upgrading, and fuel combustion. Although regions with favorable climate and productivity, such as the southwestern U.S., generally show lower GWP values, these advantages are not sufficient to offset downstream conversion, transportation, N_2O emissions, and state-specific electricity-grid impacts in most locations. Nevertheless, this regional advantage is not uniform. For example, some locations with favorable productivity, such as Texas, still show elevated GWP when biomass must be transported longer distances to the centralized biorefinery. Among the evaluated locations, Arizona is the only case that falls near the RFS threshold. This result is mainly associated with the concentration of dairy lagoon flow and the centralized biorefinery location within the same county, which minimizes biomass transportation emissions. These results suggest that meeting RFS thresholds requires not only favorable ATS productivity, but also short transport distances, lower-emission electricity inputs, reduced N_2O formation, and efficient downstream conversion.

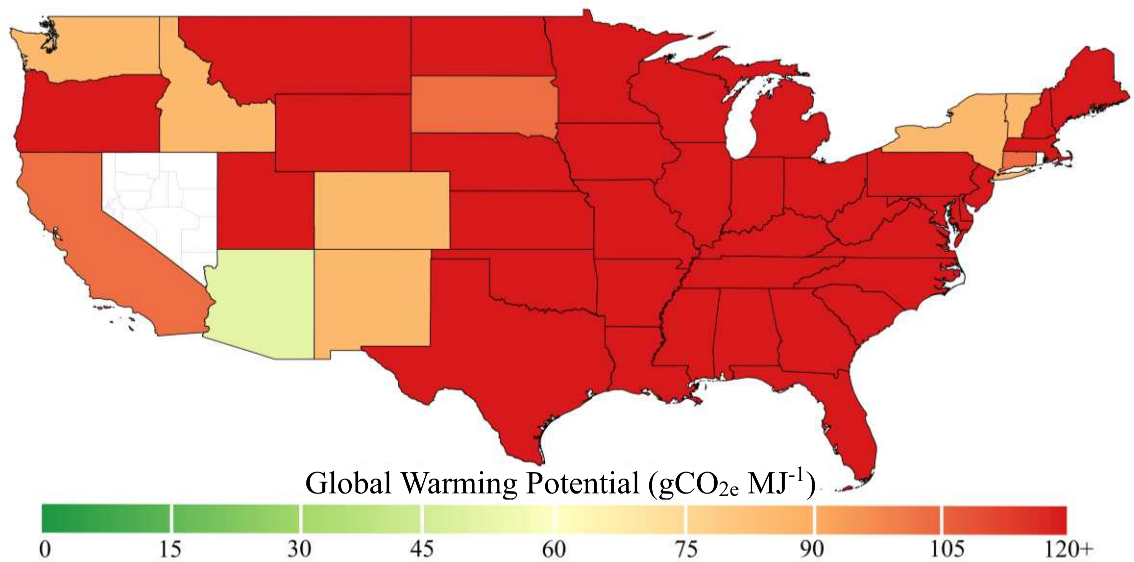

Figure 4. Full-pathway GWP across the continental United States (CONUS) for the ATS-to-renewable-diesel pathway, expressed in g CO_2e MJ^{-1}. Results include ATS cultivation, harvesting, biomass transportation, HTL processing, upgrading, and end-use fuel combustion. The Renewable Fuel Standard threshold is 45 g CO_2e MJ^{-1}. White areas represent regions with missing nutrient data or zero wastewater flow.

3.4.2 Global Warming Potential Breakdown

The state-level GWP breakdown in Figure 5 identifies the process contributions driving full-pathway emissions across representative biorefineries. Feedstock transportation was the largest contributor in most states, highlighting the burden of hauling ATS biomass to centralized HTL facilities. Electricity grid effects were also a major contributor, indicating that regional grid intensity strongly influences the overall carbon performance of the pathway. Biogenic carbon uptake during algal cultivation provides an important CO_2 removal credit during biomass growth; however, this benefit is partially offset by CO_2 released during HTL processing and upgrading, as well as end-use combustion. With biomass composition held constant across locations, conversion-related emissions remained relatively similar across states, while differences in net GWP were driven mainly by feedstock logistics, electricity inputs, and cultivation-related emissions.

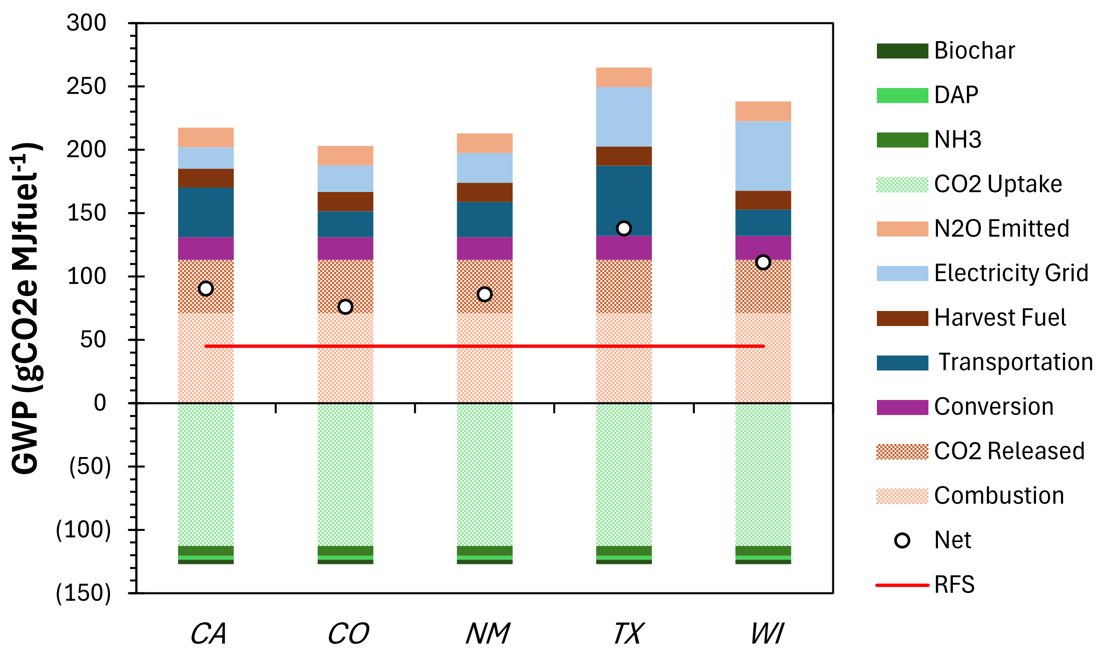

Figure 5. Breakdown of GWP for five representative biorefinery locations from ATS grown from anaerobic lagoon systems. GWP includes emissions from cultivation, transportation, conversion,

CO_2 released from aqueous and gas phases in hydrothermal liquefaction, and combustion, as well as credits from CO_2 uptake by biomass, displacement of fertilizer production (NH_3 and DAP), and carbon sequestration via biochar. Renewable Fuel Standard is marked by a red line.

Feedstock transportation emissions vary substantially across states, ranging from 20.5 g CO_2e MJ^{-1} in Colorado to 55.5 g CO_2e MJ^{-1} in Texas. Electricity-grid effects also differ by location, ranging from 16.9 g CO_2e MJ^{-1} in California to 54.8 g CO_2e MJ^{-1} in Wisconsin, with Texas also showing a high value of 47.0 g CO_2e MJ^{-1}. N_2O emissions are smaller but still relevant, contributing 15.4 g CO_2e MJ^{-1} across all five states. This is especially important for N_2O because neglecting it would underestimate the GWP burden of high-N ATS systems, where not all N removal is assimilated into biomass. These values demonstrate environmental performance of ATS-derived fuel is not uniform across deployment locations and depends strongly on site-specific logistics and electricity grids.

The GWP contribution analysis shows that life-cycle emissions are driven primarily by upstream biomass supply requirements rather than HTL conversion. Algal cultivation, biomass concentration, and feedstock transportation dominate positive burdens, while NH_3, DAP, and biochar credits provide relatively small offsets. Even after these credits, net GWP remains above the RFS threshold in all five representative states: 76.1 g CO_2e MJ^{-1} in Colorado, 85.9 g CO_2e MJ^{-1} in New Mexico, 90.5 g CO_2e MJ^{-1} in California, 111.1 g CO_2e MJ^{-1} in Wisconsin, and 138.0 g CO_2e MJ^{-1} in Texas. Texas shows the highest net GWP because it combines the largest biomass transportation burden with one of the highest electricity-related burdens. Therefore, reducing GWP would require improvements in cultivation energy use, biomass concentration, and facility logistics rather than HTL conversion alone.

3.4.3 TRACI Breakdown

The normalized TRACI breakdown for Colorado is shown in Figure 6, illustrating how the environmental performance of the ATS-to-HTL pathway varies across impact categories. The results show that no single process dominates all categories; however, feedstock transportation was one of the largest positive contributors across most impact categories. This indicates that biomass logistics represent a major environmental challenge for centralized HTL deployment. Although centralized biorefineries may provide economic advantages through economies of scale, the associated transportation burdens suggest that more distributed processing configurations, such as county-level or regional facilities, could reduce life-cycle impacts, although their economic feasibility would require further evaluation.

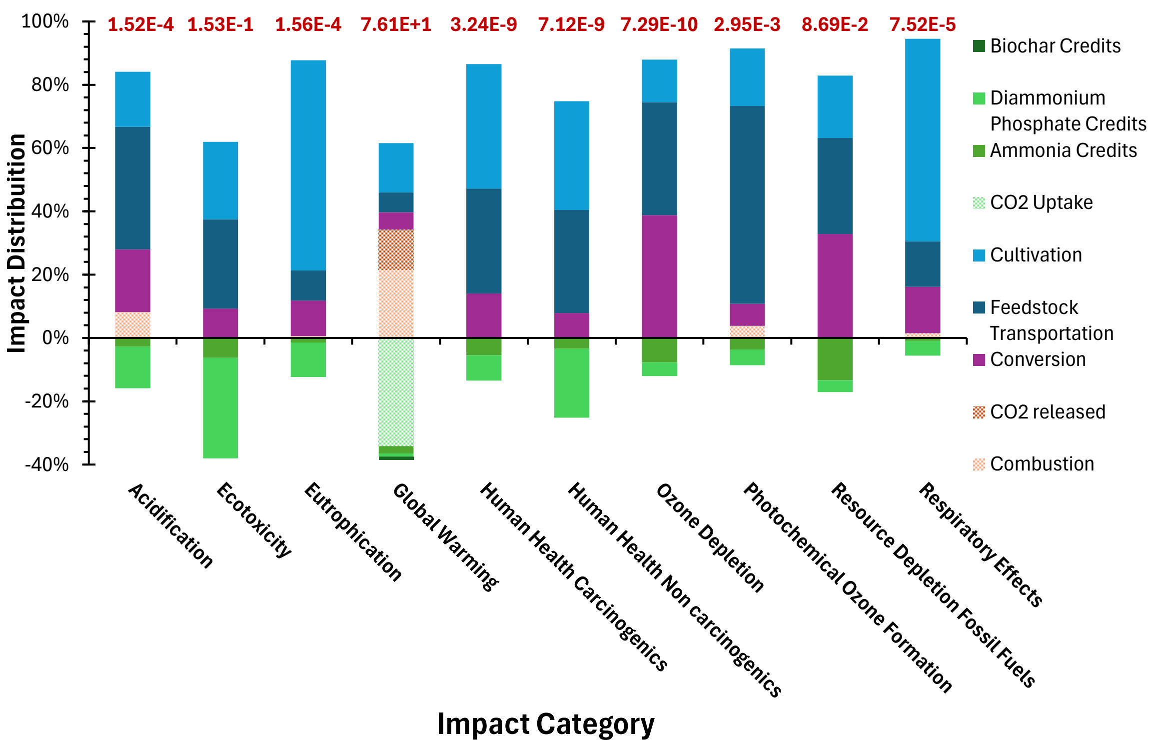

Figure 6. Normalized TRACI impact breakdown for Colorado. Bars show the relative contribution of each process stage and credit term to the total impact in each category. Positive values represent

burdens from end-use fuel combustion, biogenic CO_2 released during HTL conversion, other HTL conversion emissions, feedstock transportation, and cultivation, whereas negative values represent offsets from CO_2 uptake and coproduct credits including DAP, NH_3 and Biochar. Total impact values for each category are shown in red above the bars. All units are reported per MJ fuel: acidification (kg SO_2 eq), ecotoxicity (CTUe), eutrophication (kg N eq), global warming (g CO_2e), human health carcinogenics (CTUh), human health non-carcinogenics (CTUh), ozone depletion (kg CFC-11 eq), photochemical ozone formation (kg O_3 eq), fossil fuel resource depletion (MJ), and respiratory effects (kg $PM_{2.5}$ eq).

Cultivation-related impacts were most important for eutrophication and respiratory effects as the electricity during ATS operation carries upstream grid-related particulate and nitrogen-emission burdens, which strongly affect these TRACI categories, while feedstock transportation dominated several other categories due to distance-dependent hauling of wet biomass to centralized HTL facilities. For eutrophication, the net impact was 1.56×10^{-4} kg N eq MJ^{-1}, with cultivation accounting for 66% of the normalized contribution magnitude. HTL conversion and feedstock transportation contributed 11% and 9.5%, respectively, while coproduct credits partially offset the impact. Chen and Quinn [21], reported an eutrophication impact of 3.5×10^{-3} kg N eq MJ^{-1} for an ORP-based algae-to-HTL pathway, where the result was strongly affected by nutrient recycling assumptions. Therefore, this comparison should be interpreted as a contextual benchmark rather than a direct equivalence.

For acidification, the net impact was 1.5×10^{-4} kg SO_2 eq MJ^{-1}, with feedstock transportation contributing 39%, followed by HTL conversion (20%) and cultivation (17%). Photochemical ozone formation reached 2.95×10^{-3} kg O_3 eq MJ^{-1}, primarily driven by feedstock transportation (63%), cultivation (18%), and HTL conversion (6.9%). These values are comparable in magnitude to those reported in [21], although the contribution patterns differ because cultivation, harvesting, and HTL were assumed to be co-located, while the centralized configuration evaluated in this study increases the relative importance of biomass logistics across multiple impact categories. Therefore, reducing biomass transport distances, cultivation-related inputs, and nitrogen emissions from ATS operation represents an opportunity to further improve the environmental performance of the ATS-to-HTL pathway.

3.5 Sensitivity and uncertainty

3.5.1 TEA Sensitivity Analysis

Cultivation sensitivity results show that MBSP is most sensitive to parameters that directly affect biomass productivity and ATS cost (Appendix Figure A5.1). Under conservative cost assumptions, the baseline MBSP is \$2.75 kg algae^{-1}, and a ±20% change in light-use efficiency shifts MBSP from \$2.3 to \$3.9 kg algae^{-1}, making it the strongest cultivation driver. Feed solids fraction also has a large effect, changing MBSP from approximately \$2.2 to \$3.3 kg algae^{-1}, because solids content determines the relative amount of algal biomass and water processed downstream. ATS module cost shifts MBSP from approximately \$2.2 to \$3.2 kg algae^{-1} under conservative assumptions, while kinetic and nutrient-related parameters such as $K_{s,N}$, TN uptake, and biomass nitrogen fraction produce smaller but still meaningful changes. Under optimistic cost assumptions, the same pattern is observed, with light-use efficiency shifting MBSP from approximately \$0.27 to \$0.44 kg algae^{-1}, followed by feed solids fraction (\$0.26–0.39 kg algae^{-1}) and module cost (\$0.28–0.36 kg algae^{-1}). Overall, the cultivation sensitivity analysis indicates that improving light-use efficiency, increasing harvested solids content, and reducing ATS module costs provide the greatest opportunities to reduce biomass production cost.

Biofuel sensitivity results show that MFSP is primarily controlled by biomass price and algal composition (Appendix Figure A5.1). Under conservative assumptions, the baseline MFSP is \$40.2 LGE^{-1}, and a ±20% change in biomass price shifts MFSP from \$33 to \$48 LGE^{-1}, making upstream biomass cost the dominant fuel-cost driver. Protein fraction is the next most influential parameter, varying MFSP from \$37 to \$44 LGE^{-1}, followed by lipid fraction, which shifts MFSP from about \$40 to \$43 LGE^{-1}. Under optimistic assumptions, biomass price remains the dominant parameter, shifting MFSP from approximately \$6.6 to \$8.6 LGE^{-1}, followed by protein fraction (\$6.9–8.2 LGE^{-1}) and lipid fraction (\$7.5–8.0 LGE^{-1}). Overall, the biofuel sensitivity analysis indicates that final fuel economics are driven more strongly by upstream biomass cost and feedstock composition than by HTL or upgrading equipment costs.

3.5.2 TEA Monte Carlo Analysis

To evaluate how parameter uncertainty affects economic outcomes, Monte Carlo analysis is applied to Weld County cultivation and propagated through the Colorado HTL model, as shown in Figure 7. The analysis evaluates the resulting distributions for MBSP, MWSP, MFSP under conservative and optimistic cost assumptions, capturing uncertainty in biomass production cost, feedstock availability, and algal composition without nutrient credits.

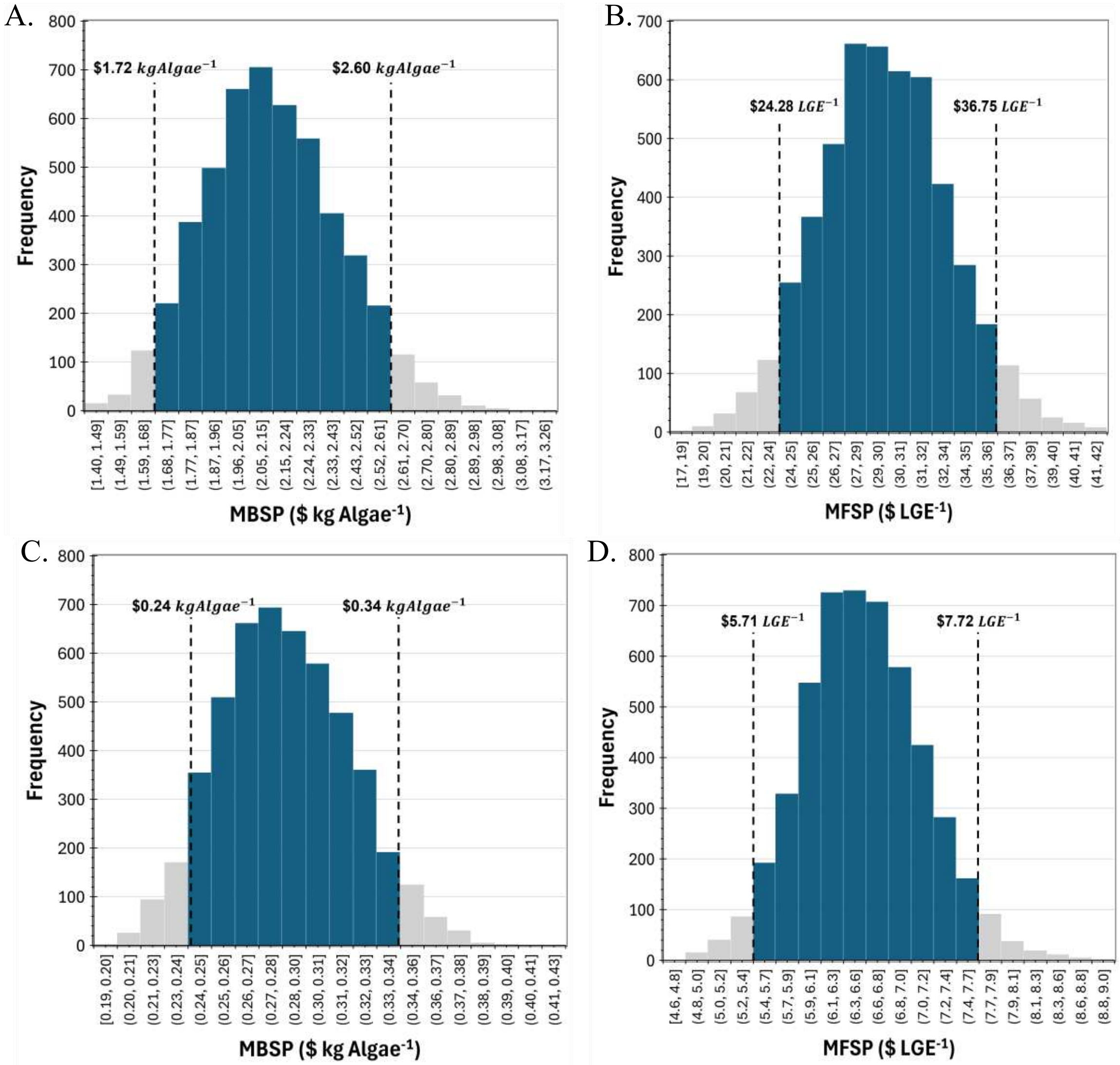

Figure 7. Monte Carlo histograms for cultivation MBSP and HTL MFSP under conservative and optimistic scenarios with no credits. A) Conservative MBSP. B) Conservative MFSP. C) Optimistic MBSP. D) Optimistic MFSP. Blue bars show the central 90% of the simulated output distribution, defined by the 5th and 95th percentiles, whereas gray bars indicate the lower and upper tails outside this interval.

For cultivation, MBSP ranged from \$1.72 to \$2.60 kg wet algae slurry^{-1} under conservative costs and from \$0.24 to \$0.34 kg wet algae slurry^{-1} under optimistic assumptions, representing the 90% interval from the Monte Carlo analysis (Figure 7). Total algae feedstock averages 4,140 ±

814 tonne wet algae slurry^{-1}, while MWSP ranged from \$4.53 to \$6.30 m^{-3} under conservative assumptions and from \$0.60 to \$0.84 m^{-3} under optimistic assumptions (Appendix Figure A11). These results provide confidence that improved cultivation economics can support the water-treatment and nutrient-recovery function of ATS systems.

When cultivation uncertainty was propagated into the Colorado HTL model, MFSP ranged from \$24.28 to \$36.75 LGE^{-1} (\$91.9 to \$139.1 GGE^{-1}) under conservative assumptions and from \$5.71 to \$7.72 LGE^{-1} (\$21.6 to \$29.2 GGE^{-1}) under optimistic assumptions, representing the 90% interval from the Monte Carlo analysis (Figure 7). These values remain above the target fuel selling price of \$0.98 LGE^{-1} (\$3.71 GGE^{-1}), even under optimistic assumptions. Overall, the Monte Carlo analysis shows that uncertainty in the selected variables does not change the main economic conclusion: renewable diesel production alone is not economically competitive for ATS-derived biomass without additional value from nutrient credits. Therefore, the pathway is better supported when ATS biomass is evaluated as part of an integrated nutrient-recovery system rather than as a fuel-only feedstock.

3.5.3 LCA Sensitivity and Monte Carlo Analysis

LCA sensitivity results for Weld County show that GWP is most strongly influenced by total feed, protein fraction, ATS electricity demand, and transport distance (Appendix Figure A5.2A). Smaller but still relevant effects are observed for harvestable algae, carbohydrate fraction, lipid fraction, and N_2O emissions. These results indicate that environmental performance is controlled not only by HTL conversion assumptions, but also by upstream biomass quantity, composition, electricity demand, and logistics. The strong influence of total feed and protein fraction shows that biomass characteristics can alter GWP by affecting HTL yields and the balance of process emissions, while ATS electricity demand and transport distance remain key environmental hotspots.

The LCA Monte Carlo results for Weld County show a relatively concentrated GWP distribution (Appendix Figure A5.2B), with a central 90% confidence interval from 66.62 to 85.67 g CO_2e MJ^{-1}. This range remains above the RFS threshold, indicating that simultaneous variation in sensitive parameters does not change the conclusion that the representative case exceeds low-carbon fuel requirements. Meaningful GWP reductions would therefore require combined improvements in electricity demand, transport distance, N-related emissions, biomass composition, and feedstock requirements. Overall, these results show that future improvements should be evaluated not only by their effect on fuel price, but also by their ability to reduce full-pathway GWP.

3.6 Deployment implications

The results indicate that lagoon-ATS systems are more suitable as a nutrient-recovery technology than as large-scale renewable diesel replacement pathways. Although ATS-derived biomass can be converted to renewable diesel, fuel output remains small relative to national transportation fuel demand. Therefore, fuel production is better interpreted as a potential co-product of lagoon treatment rather than the primary deployment driver. The main deployment constraint is also water availability rather than nutrient availability. Anaerobic lagoons contain large total volumes, but long hydraulic retention times and permanent treatment-zone requirements limit the fraction of water that can be withdrawn for daily ATS operation [10].

The end use of ATS-lagoon biomass depends on its composition, environmental regulations, market demand, and site-specific deployment constraints. When nutrient removal is the primary objective, harvested biomass should be treated as a co-product rather than the main product. Depending on regional conditions, lower-value uses such as land-applied fertilizer, soil amendments, or biochar may be more appropriate than fuel production because they can displace synthetic fertilizer demand and support carbon sequestration without requiring a dedicated fuel-processing facility [85]. Future work should evaluate land availability and spatial constraints more explicitly because county-level aggregation may oversimplify local dairy clustering, available land for ATS deployment, and biomass logistics.

Environmental deployment strategies should address two main burdens identified in the LCA: biomass logistics and nitrogen emissions. Centralized state-level HTL facilities may improve economies of scale but increase hauling distances, especially in large or dispersed dairy states. Regional or modular HTL facilities could reduce feedstock hauling distances, as previous modular HTL studies have identified transportation costs and optimal plant scale as key factors affecting biofuel pricing [86]. In parallel, high-nutrient ATS systems should include N_2O monitoring or mitigation strategies, especially when designed for intensive N removal. The LCA results show that N emissions can influence eutrophication and GWP outcomes, indicating that nutrient recovery benefits should be evaluated together with potential emission tradeoffs. These results suggest that deployment strategies should prioritize reducing biomass transport burdens while managing N emissions to improve the environmental performance of ATS-to-HTL systems.

3.7 Model limitations

The main limitations of this model relate to the assumed regulatory and economic value of nutrient removal, lagoon-derived water and biofilm conditions, and extrapolation from controlled indoor experiments to field-scale deployment. This study assumes a future policy context in which stricter nutrient targets, environmental penalties, or incentive programs create value for reducing

N and P in anaerobic lagoon effluent. Although lagoon effluent is often managed within the farm system rather than regulated as a fully polished discharge, increasing concern over nutrient losses to groundwater, surface waters, and agricultural soils could drive demand for cost-competitive nutrient-recovery technologies. Under this assumption, lagoon-based ATS systems are evaluated not only as a biomass-production pathway, but as a potential treatment strategy for farms and agencies seeking to reduce nutrient losses and protect surrounding water resources.

Lagoon-derived water quality is another important limitation as the model does not explicitly resolve turbidity, color, or volatile suspended solids (VSS) related light attenuation. These effects are expected to be limited in shallow ATS flow-ways because laboratory water-film thickness is estimated at 12.7–25.4 mm (0.5–1.0 in), consistent with HydroMentia guidance that ATS water depths are generally below 25.4 mm (1 in) [54]. Lagoon-derived organic matter could also support heterotrophic biofilm growth; however, based on diluted BOD_5 and typical heterotrophic yields of 0.4–0.6 g VSS g^{-1} BOD_5 removed [36], this contribution was estimated as only 2.1-3.2 g VSS m^{-2} d^{-1}. ATS biomass is a mixed algal–microbial biofilm; therefore, the estimated VSS contribution could include heterotrophic bacteria, cyanobacteria, extracellular polymeric substances, retained organic solids, and algae. The algal fraction of this contribution was not experimentally determined; therefore, organic-carbon-supported growth was not included as a separate algal productivity term in the base model. This avoids overstating algae-derived fuel feedstock, but may underestimate total harvested solids where heterotrophic growth is substantial.

Finally, field-scale deployment is simplified through modular HydroMentia-based ATS area constraints [54] and regional productivity adjustments based on climate conditions. This approach limits extrapolation beyond existing design practice but does not resolve longitudinal nutrient, light, or biofilm gradients in longer field-scale systems. It also treats temperature as an operating-window constraint rather than a continuous growth-rate function. Because kinetic and productivity parameters are derived from controlled indoor experiments and extrapolated to outdoor county-level conditions, the model may not fully capture site-specific variability in temperature, light exposure, hydrodynamics, biofilm ecology, and lagoon effluent composition. Future work should evaluate field-scale gradients, start-up periods, downtime, culture stability, and seasonal performance losses, and should incorporate a temperature-dependent growth function, such as a cardinal temperature model [87], to capture minimum, optimum, and maximum operating temperatures and improve seasonal productivity estimates under outdoor conditions. Biomass composition is another key uncertainty affecting harvested algae utilization. The measured lipid content of 5.2% is low for fuel production, which may limit HTL fuel yields and supports the need for additional biomass characterization [56]. Together, these limitations indicate that field validation with real lagoon effluent is needed to refine productivity, treatment performance, and biomass utilization estimates.

4. CONCLUSIONS

This study demonstrates that lagoon-based ATS systems are more valuable as a nutrient-recovery technology than as a renewable diesel replacement pathway. Using a spatially resolved framework that links high-nutrient dairy lagoon effluent, Monod-based uptake kinetics, CONUS dairy wastewater availability, modular ATS design, and HTL conversion, the model evaluates both the treatment value and fuel potential of ATS-derived biomass. The results show that deployment is constrained primarily by water availability rather than nutrient loading, because lagoon withdrawal, recirculation, and harvest timing limit daily flow through the system. Experimental results also indicate that nutrient removal is not driven by biomass assimilation alone, with approximately 42% of TN and TP removal associated with algal biomass and slough and the remaining 58% attributed to additional removal pathways. Economically, renewable diesel production from ATS biomass is not competitive without recognizing the value of nutrient removal. Under conservative assumptions, required N and P credits are below conventional treatment costs in 30% and 65% of locations, respectively, while optimistic assumptions increase this to 96% of locations for both nutrients. These results indicate that ATS deployment is most favorable when nutrient removal is treated as the primary service and biomass is treated as a co-product. The LCA further shows that environmental performance depends strongly on biomass logistics and N emissions, with centralized HTL increasing transportation burdens. Future deployment should prioritize water availability, regional biomass use, N_2O monitoring, and field validation with real lagoon effluent. Together, these findings suggest that future ATS deployment should be designed around nutrient-removal value, local biomass use, and reduced environmental burdens rather than maximizing fuel output alone.

5. REFERENCES

[1] FAO, “Livestock and environment statistics: manure and greenhouse gas emissions. Global, regional and country trends, 1990–2018,” *FAOSTAT Analytical Brief Series No. 14*, 2020.

[2] U.S. Environmental Protection Agency, “Inventory of U.S. Greenhouse Gas Emissions and Sinks: 1990–2022,” Washington, DC, EPA 430-R-24-004, Apr. 2024. [Online]. Available: https://www.epa.gov/system/files/documents/2024-04/us-ghg-inventory-2024-main-text_04-18-2024.pdf

[3] “Funding On-Farm Anaerobic Digestion,” EPA, Sep. 2012.

[4] Guidehouse Inc., “Renewable Natural Gas Economic Impact Analysis,” RNG Coalition, Dec. 2024.

[5] “LFG Energy Project Development Handbook,” Sep. 2012.

[6] W. Shuros and C. Hartog, “Alternative Technologies for Municipal Solid Waste,” Foth Infrastructure & Environment, LLC, Lake Elmo, MN, Jul. 2013. [Online]. Available: https://www.ourenergypolicy.org/wp-content/uploads/2014/07/alternative.pdf

[7] “Part 651 – Agricultural Waste Management Field Handbook,” Title 210 – National Engineering Handbook, Sep. 2025.

[8] “Conservation Practice Standard Waste Treatment Lagoon (Code 359),” 2017.

[9] “Methodology for Estimating CH4 Emissions from Enteric Fermentation,” U.S. Environmental Protection Agency.

[10] “Lagoons for Storage/Treatment of Dairy Waste,” University of Missouri Extension, Columbia, MO, WQ304. [Online]. Available: https://extension.missouri.edu/publications/wq304

[11] M. Sharara, “How Does Nitrogen Move Through a Swine Farm with a Lagoon-Sprayfield System?,” NC State Extension, AG-927, Jun. 2022. [Online]. Available: https://content.ces.ncsu.edu/how-does-nitrogen-move-through-a-swine-farm-with-a-lagoon-sprayfield-system

[12] W. Adey, P. Kangas, and W. Mulbry, “Algal Turf Scrubbing: Cleaning Surface Waters with Solar Energy while Producing a Biofuel,” vol. 61, no. 6, pp. 434–441, Jun. 2011, doi: https://doi.org/10.1525/bio.2011.61.6.5.

[13] Hydromentia, “Preliminary Engineering Assessment for a Comprehensive Algal Turf Scrubber Based Nutrient Control Program for the Suwannee River in Florida.”

[14] E. Westhead, C. Pizarro, and W. Mulbry, “DEVELOPMENT OF ALGAL TURF SCRUBBERS TO TREAT DAIRY MANURE,” Mar. 2001. [Online]. Available: https://www.ars.usda.gov/research/publications/publication/?seqNo115=121605

[15] Hydromentia, “Taylor Creek Algal Turf Scrubber® Nutrient Recovery Facility for Phosphorus and Nitrogen Control.” [Online]. Available: https://hydromentia.com/case-studies/taylor-creek-algal-turf-scrubber/

[16] B. T. Higgins and A. Kendall, “Life Cycle Environmental and Cost Impacts of Using an Algal Turf Scrubber to Treat Dairy Wastewater,” *J of Industrial Ecology*, vol. 16, no. 3, pp. 436–447, Jun. 2012, doi: 10.1111/j.1530-9290.2011.00427.x.

[17] M. Biddy, R. Davis, S. Jones, and Z. Yunhua, “Whole Algae Hydrothermal Liquefaction Technology Pathway,” *Technical Report NREL/TP-5100-58051 PNNL-22314*, Mar. 2013.

[18] P. Valdez, "Hydrothermal Liquefaction Model Development," *DOE Bioenergy Technologies Office (BETO) 2023 Project Peer Review Advanced Algal Systems Program*, 2023.

[19] A. Ryland *et al.*, "Techno-economic analysis and life cycle assessment of algal turf scrubbers treating wastewater effluent for renewable diesel production," *Algal Research*, vol. 93, p. 104459, Jan. 2026, doi: 10.1016/j.algal.2025.104459.

[20] A. B. Banks, P. H. Chen, C. Quiroz-Arita, R. W. Davis, and J. C. Quinn, "Geographically-resolved evaluation of the economic and environmental services from renewable diesel derived from attached algae flow-ways across the United States," *Algal Research*, vol. 72, p. 103100, May 2023, doi: 10.1016/j.algal.2023.103100.

[21] P. H. Chen and J. C. Quinn, "Microalgae to biofuels through hydrothermal liquefaction: Open-source techno-economic analysis and life cycle assessment," *Applied Energy*, vol. 289, p. 116613, May 2021, doi: 10.1016/j.apenergy.2021.116613.

[22] "Agricultural Waste Characteristics," USDA NRCS, Washington, D.C, Chapter 4, 2008.

[23] C. Pizarro, W. Mulbry, D. Blersch, and P. Kangas, "An economic assessment of algal turf scrubber technology for treatment of dairy manure effluent," *Ecological Engineering*, vol. 26, no. 4, pp. 321–327, Jul. 2006, doi: 10.1016/j.ecoleng.2005.12.009.

[24] W. Mulbry, S. Kondrad, C. Pizarro, and E. Kebede-Westhead, "Treatment of dairy manure effluent using freshwater algae: Algal productivity and recovery of manure nutrients using pilot-scale algal turf scrubbers," *Bioresource Technology*, vol. 99, no. 17, pp. 8137–8142, Nov. 2008, doi: 10.1016/j.biortech.2008.03.073.

[25] A. W. Mayo and E. E. Hanai, “Dynamics of Nitrogen Transformation and Removal in a Pilot High Rate Pond,” *JWARP*, vol. 06, no. 05, pp. 433–445, 2014, doi: 10.4236/jwarp.2014.65043.

[26] J. J. Beaulieu *et al.*, “Nitrous oxide emission from denitrification in stream and river networks,” *Proc. Natl. Acad. Sci. U.S.A.*, vol. 108, no. 1, pp. 214–219, Jan. 2011, doi: 10.1073/pnas.1011464108.

[27] Environmental Protection Agency and AWWA, “Nitrification,” Aug. 2002.

[28] “N2O EMISSIONS FROM MANAGED SOILS, AND CO2 EMISSIONS FROM LIME AND UREA APPLICATION,” IPCC, 2006 IPCC Guidelines for National Greenhouse Gas Inventories, 2006.

[29] G. Mancuso *et al.*, “Performance of lagoon and constructed wetland systems for tertiary wastewater treatment and potential of reclaimed water in agricultural irrigation,” *Journal of Environmental Management*, vol. 348, p. 119278, Dec. 2023, doi: 10.1016/j.jenvman.2023.119278.

[30] J. Clark, J. Gerwing, and R. Gelderman, “Fertilizer Recommendations Guide,” 2005.

[31] F. Muabuay, S. Sharvelle, M. Ghorbanian, L. Graham, and G. Johnson, “Assessing the performance of a novel membrane system to generate recycled water and solids for methane generation from flushed dairy manure,” *Journal of Environmental Chemical Engineering*, vol. 13, no. 6, p. 119906, Dec. 2025, doi: 10.1016/j.jece.2025.119906.

[32] M. Sophocleous, M. A. Townsend, F. Vocasek, L. Ma, and A. Kc, “Soil Nitrogen Balance under Wastewater Management: Field Measurements and Simulation Results,” *J of Env Quality*, vol. 38, no. 3, pp. 1286–1301, May 2009, doi: 10.2134/jeq2008.0318.

[33] Environmental Protection Agency, “Concentrated animal feeding operations,” Jun. 2025, [Online]. Available: https://www.ecfr.gov/current/title-40/chapter-I/subchapter-D/part-122/subpart-B/section-122.23

[34] U.S. Department of Agriculture, “2022 Census Dairy Data,” 2022. [Online]. Available: https://quickstats.nass.usda.gov/

[35] Environmental Protection Agency, “Annex 3: Inventory of U.S. Greenhouse Gas Emissions and Sinks,” 2022.

[36] B. E. Rittmann and P. L. McCarty, *Environmental Biotechnology: Principles and Applications*, 2nd Edition. New York: McGraw-Hill Education, 2020. [Online]. Available: https://www.accessengineeringlibrary.com/content/book/9781260441604

[37] Environmental Protection Agency, “IWMS - Entire Farm Data Irrigation Rates,” vol. Table 7, 2023.

[38] Q. Zhou *et al.*, “Nutrients removal mechanisms in high rate algal pond treating rural domestic sewage in East China,” *Water Supply*, vol. 6, no. 6, pp. 43–50, Dec. 2006, doi: 10.2166/ws.2006.956.

[39] L. Delgadillo-Mirquez, F. Lopes, B. Taidi, and D. Pareau, “Nitrogen and phosphate removal from wastewater with a mixed microalgae and bacteria culture,” *Biotechnology Reports*, vol. 11, pp. 18–26, Sep. 2016, doi: 10.1016/j.btre.2016.04.003.

[40] F. El Hafiane and B. El Hamouri, “Anaerobic reactor/high rate pond combined technology for sewage treatment in the Mediterranean area,” *Water Science and Technology*, vol. 51, no. 12, pp. 125–132, Jun. 2005, doi: 10.2166/wst.2005.0445.

[41] W. H. Adey, M. S. S. John, F. B. Green, and W. J. Oswald, “Phosphorus removal from wastewater using an algal turf scrubber,” *Wat Sci. tech*, vol. 33, pp. 191–198, 1996, doi: https://doi.org/10.2166/wst.1996.0138.

[42] R. Craggs, J. Park, S. Heubeck, and D. Sutherland, “High rate algal pond systems for low-energy wastewater treatment, nutrient recovery and energy production,” *New Zealand Journal of Botany*, vol. 52, no. 1, pp. 60–73, Mar. 2014, doi: 10.1080/0028825X.2013.861855.

[43] W. K. Dodds, “THE ROLE OF PERIPHYTON IN PHOSPHORUS RETENTION IN SHALLOW FRESHWATER AQUATIC SYSTEMS,” *Journal of Phycology*, vol. 39, no. 5, pp. 840–849, Oct. 2003, doi: 10.1046/j.1529-8817.2003.02081.x.

[44] W. H. Adey *et al.*, “Algal turf scrubber (ATS) floways on the Great Wicomico River, Chesapeake Bay: productivity, algal community structure, substrate and chemistry[1],” *Journal of Phycology*, vol. 49, no. 3, pp. 489–501, Jun. 2013, doi: 10.1111/jpy.12056.

[45] L. G. Ramírez Mérida and R. A. Rodríguez Padrón, “Application of microalgae in wastewater: opportunity for sustainable development,” *Frontiers in Environmental Science*, vol. Volume 11-2023, 2023, [Online]. Available: https://www.frontiersin.org/journals/environmental-science/articles/10.3389/fenvs.2023.1238640

[46] D. F. Toerien and C. H. Huang, “Algal growth prediction using growth kinetic constants,” *Water Research*, vol. 7, no. 11, pp. 1673–1681, Nov. 1973, doi: 10.1016/0043-1354(73)90135-8.

[47] A. Thornton, “Modeling and optimization of algae growth,” *CASA Report*, vol. 1059, Jan. 2010.

[48] H.-Y. Kim, “Statistical notes for clinical researchers: simple linear regression 1 – basic concepts,” *Restor Dent Endod*, vol. 43, no. 2, p. e21, Apr. 2018, doi: 10.5395/rde.2018.43.e21.

[49] Hydromentia, “S-154 Pilot Single Stage Algal Turf Scrubber® (ATSTM) Final Report,” *South Florida Water Management District Under Contract No. C-13933*, Mar. 2025.

[50] R. W. Davis, “Attached Periphytic Algae Production & Analysis,” *DOE Bioenergy Technologies Office (BETO) 2021 Project Peer Review*, Mar. 2021.

[51] J. Hoffman, R. C. Pate, T. Drennen, and J. C. Quinn, “Techno-economic assessment of open microalgae production systems,” *Algal Research*, vol. 23, pp. 51–57, Apr. 2017, doi: 10.1016/j.algal.2017.01.005.

[52] D. Pfost, C. Fulhage, and D. Rastorfer, “Anaerobic Lagoons for Storage/Treatment of Livestock Manure,” *MU Extension EQ 387*.

[53] A. M. Schmidt, “Managing Earthen Manure Storage Basins During Drought,” *The Board of Regents of the University of Nebraska on behalf of the University of Nebraska–Lincoln Extension*, 2013, [Online]. Available: http://extension.unl.edu/publications

[54] Hydromentia, “Algal Turf Scrubber Features and Benefits.” [Online]. Available: https://hydromentia.com/algal-turf-scrubber/benefits/

[55] K. DeRose, C. DeMill, R. W. Davis, and J. C. Quinn, “Integrated techno economic and life cycle assessment of the conversion of high productivity, low lipid algae to

renewable fuels," *Algal Research*, vol. 38, p. 101412, Mar. 2019, doi: 10.1016/j.algal.2019.101412.

[56] P. J. Valdez, V. J. Tocco, and P. E. Savage, "A general kinetic model for the hydrothermal liquefaction of microalgae," *Bioresource Technology*, vol. 163, pp. 123–127, Jul. 2014, doi: 10.1016/j.biortech.2014.04.013.

[57] Internal Revenue Service (IRS), "How To Depreciate Property," Mar. 2026. [Online]. Available: https://www.irs.gov/pub/irs-pdf/p946.pdf

[58] S. Jenkins, "Chemical Engineering Plant Cost Index Annual Average, Chem. Eng." [Online]. Available: https://www.chemengonline.com/pci-home

[59] U.S. Bureau of Labor Statistics, "Producer Price Index by Commodity: Chemicals and Allied Products: Basic Inorganic Chemicals [WPU0613]," 2025. [Online]. Available: https://fred.stlouisfed.org/series/WPU0613

[60] U.S. Bureau of Labor Statistics, "Employment, Hours, and Earnings from the Current Employment Statistics survey (National), Series ID: CEU3232500008." [Online]. Available: https://data.bls.gov/cgi-bin/srgate

[61] R. Davis, "BETO 2021 Peer Review: Algal Biofuels Techno-Economic Analysis 1.3.5.200," *National Renewable Energy Laboratory Advanced Algal Systems Session*, 2021.

[62] K. K. DeRose, R. W. Davis, E. A. Monroe, and J. C. Quinn, "Economic viability of proactive harmful algal bloom mitigation through attached algal growth," *Journal of Great Lakes Research*, vol. 47, no. 4, pp. 1021–1032, Aug. 2021, doi: 10.1016/j.jglr.2021.04.011.

[63] U.S. Department of Agriculture, "Fiscal Year 2019 USDA Budget Summary," 2019. Accessed: Feb. 17, 2026. [Online]. Available: https://www.usda.gov/sites/default/files/documents/usda-fy19-budget-summary.pdf

[64] C. W. W. C. C. and T. R. S. Wiegand, "Cost of Urban Runoff Controls," American Society of Civil Engineers, 1986.

[65] U.S. Energy Information Administration (EIA), "Electric Power Monthly." [Online]. Available: https://www.eia.gov/electricity/monthly/epm_table_grapher.php?t=epmt_5_6_a

[66] R. J. Frei *et al.*, "Limited progress in nutrient pollution in the U.S. caused by spatially persistent nutrient sources," *PLOS ONE*, vol. 16, no. 11, p. e0258952, Nov. 2021, doi: 10.1371/journal.pone.0258952.

[67] M. Norris *et al.*, "Predicting nitrogen supply from dairy effluent applied to contrasting soil types," *New Zealand Journal of Agricultural Research*, vol. 62, no. 4, pp. 438–456, Dec. 2019, doi: 10.1080/00288233.2018.1508478.

[68] Parliamentary Counsel Office of New Zealand, "Resource Management Act 1991," Wellington, New Zealand, Feb. 2026.

[69] DLA Piper, "Significant fine for environmental offending." [Online]. Available: https://www.dlapiper.com/en/insights/publications/2024/11/significant-fine-for-environmental-offending

[70] M. Simon-Várhelyi, C. Tomoiagă, M. A. Brehar, and V. M. Cristea, "Dairy wastewater processing and automatic control for waste recovery at the municipal wastewater treatment plant based on modelling investigations," *Journal of*

Environmental Management, vol. 287, p. 112316, Jun. 2021, doi: 10.1016/j.jenvman.2021.112316.

[71] B. J. Limb, J. C. Quinn, A. Johnson, R. B. Sowby, and E. Thomas, "The potential of carbon markets to accelerate green infrastructure based water quality trading," *Commun Earth Environ*, vol. 5, no. 1, p. 185, Apr. 2024, doi: 10.1038/s43247-024-01359-x.

[72] U.S. Energy Information Administration (EIA), "U.S. Gasoline and Diesel Retail Prices." Accessed: Mar. 05, 2026. [Online]. Available: https://www.eia.gov/dnav/pet/pet_pri_gnd_dcus_nus_w.htm

[73] "ecoinvent Version 3.11." Accessed: Feb. 11, 2026. [Online]. Available: https://ecoinvent.org/ecoinvent-v3-11/

[74] J. C. Bare, "Traci," *Journal of Industrial Ecology*, vol. 6, no. 3–4, pp. 49–78, Jul. 2002, doi: 10.1162/108819802766269539.

[75] A. S. Zurano, C. G. Serrano, F. G. Acién-Fernández, J. M. Fernández-Sevilla, and E. Molina-Grima, "Modelling of photosynthesis, respiration, and nutrient yield coefficients in Scenedemus almeriensis culture as a function of nitrogen and phosphorus," *Appl Microbiol Biotechnol*, vol. 105, no. 19, pp. 7487–7503, Oct. 2021, doi: 10.1007/s00253-021-11484-8.

[76] L. Xin, H. Hong-ying, G. Ke, and S. Ying-xue, "Effects of different nitrogen and phosphorus concentrations on the growth, nutrient uptake, and lipid accumulation of a freshwater microalga Scenedesmus sp.," *Bioresource Technology*, vol. 101, no. 14, pp. 5494–5500, Jul. 2010, doi: 10.1016/j.biortech.2010.02.016.

[77] E. Sforza, M. Pastore, E. Barbera, and A. Bertucco, "Respirometry as a tool to quantify kinetic parameters of microalgal mixotrophic growth," *Bioprocess Biosyst Eng*, vol. 42, no. 5, pp. 839–851, May 2019, doi: 10.1007/s00449-019-02087-9.

[78] J. Hu, W. Meng, Y. Su, C. Qian, and W. Fu, "Emerging technologies for advancing microalgal photosynthesis and metabolism toward sustainable production," *Front. Mar. Sci.*, vol. 10, p. 1260709, Oct. 2023, doi: 10.3389/fmars.2023.1260709.

[79] D. C. Elliott, "Review of recent reports on process technology for thermochemical conversion of whole algae to liquid fuels," *Algal Research*, vol. 13, pp. 255–263, Jan. 2016, doi: 10.1016/j.algal.2015.12.002.

[80] L. Wang, Y. Li, M. Sommerfeld, and Q. Hu, "A flexible culture process for production of the green microalga Scenedesmus dimorphus rich in protein, carbohydrate or lipid," *Bioresource Technology*, vol. 129, pp. 289–295, Feb. 2013, doi: 10.1016/j.biortech.2012.10.062.

[81] Y. Gong *et al.*, "Microalgae Scenedesmus sp. as a potential ingredient in low fishmeal diets for Atlantic salmon (Salmo salar L.)," *Aquaculture*, vol. 501, pp. 455–464, Feb. 2019, doi: 10.1016/j.aquaculture.2018.11.049.

[82] IEA Bioenergy, "State of Technology Review – Algae Bioenergy," Jan. 2017.

[83] U.S. Energy Information Administration (EIA), "Gasoline explained." [Online]. Available: https://www.eia.gov/energyexplained/gasoline/use-of-gasoline.php

[84] U.S. Environmental Protection Agency, "Overview of the Renewable Fuel Standard Program." [Online]. Available: https://www.epa.gov/renewable-fuel-standard-program/overview-renewable-fuel-standard-program

[85] S. Gurau, M. Imran, and R. L. Ray, “Algae: A cutting-edge solution for enhancing soil health and accelerating carbon sequestration – A review,” *Environmental Technology & Innovation*, vol. 37, p. 103980, Feb. 2025, doi: 10.1016/j.eti.2024.103980.

[86] M. Shahabuddin, E. Italiani, A. R. Teixeira, N. Kazantzis, and M. T. Timko, “Roadmap for Deployment of Modularized Hydrothermal Liquefaction: Understanding the Impacts of Industry Learning, Optimal Plant Scale, and Delivery Costs on Biofuel Pricing,” *ACS Sustainable Chem. Eng.*, vol. 11, no. 2, pp. 733–743, Jan. 2023, doi: 10.1021/acssuschemeng.2c05982.

[87] L. Rosso, J. R. Lobry, and J. P. Flandrois, “An Unexpected Correlation between Cardinal Temperatures of Microbial Growth Highlighted by a New Model,” *Journal of Theoretical Biology*, vol. 162, no. 4, pp. 447–463, Jun. 1993, doi: 10.1006/jtbi.1993.1099.

APPENDIX A

A.1 Supplementary Figures

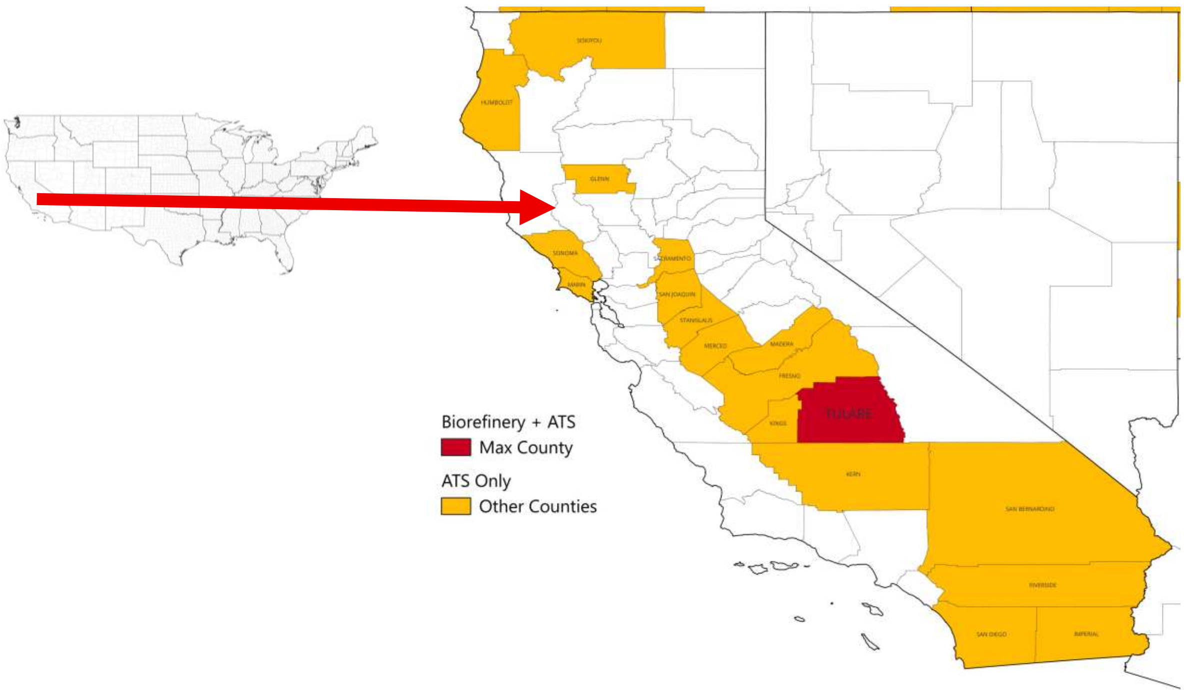

Figure A1. Tulare, California identified on the map of the continental United States. A zoomed-in view of the County region showing the locations of Anaerobic lagoons with ATS sites and biorefinery.

A.

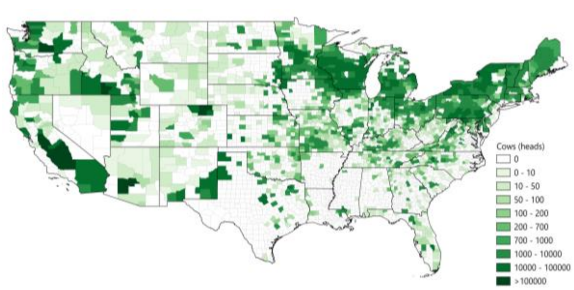

B.

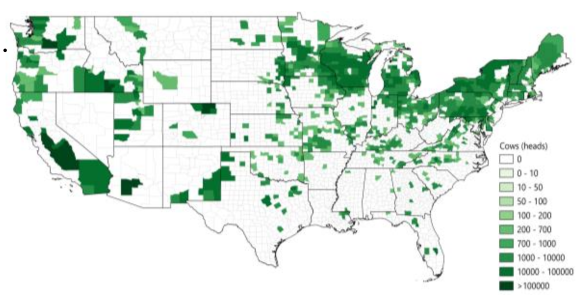

Figure A2. A) Reported values of dairy cattle per county by USDA [1] B) Possible Anaerobic Lagoons per county according to EPA [2].

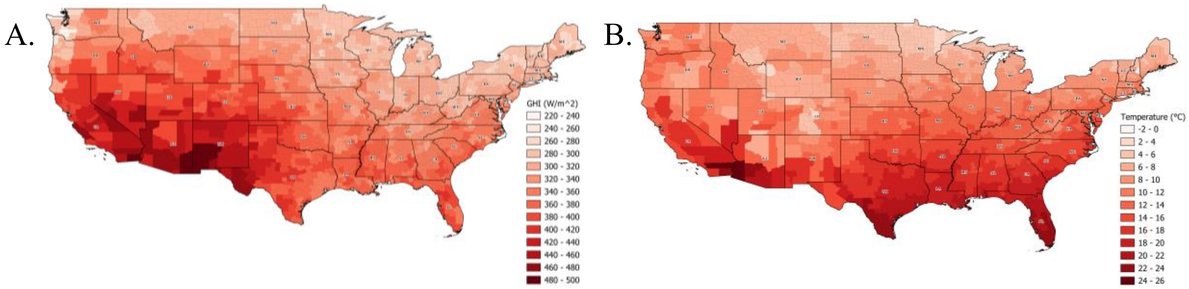

Figure A3. Spatial distribution of A) Global horizontal irradiance (GHI), expressed in W m^{-2}. B) Temperature, expressed in °C. Parameters were obtained from Banks et al. [4]. White areas indicate regions with missing data or locations excluded from the analysis.

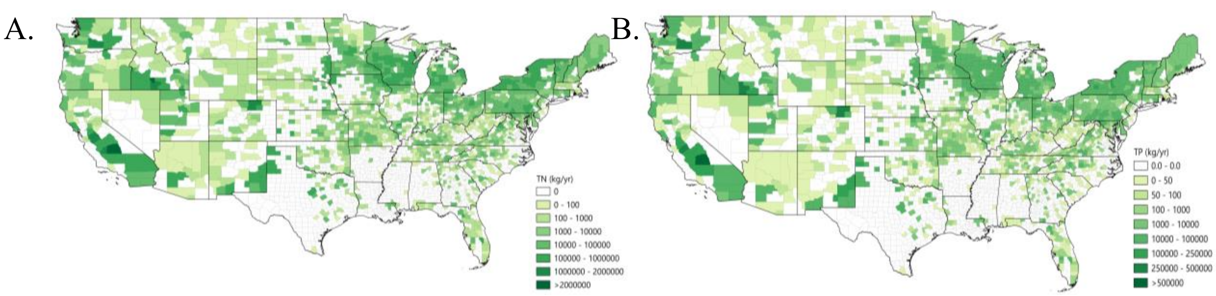

Figure A4. A) Average annual nitrogen (N) loading, expressed in kg yr^{-1}, estimated from county-level dairy cow data from the USDA Census of Agriculture 2022 [3]. B) Average annual phosphorus (P) loading, expressed in kg yr^{-1}, estimated from the same USDA Census 2022 dairy data [3]. White areas in both maps represent regions with missing data or zero reported dairy cattle.

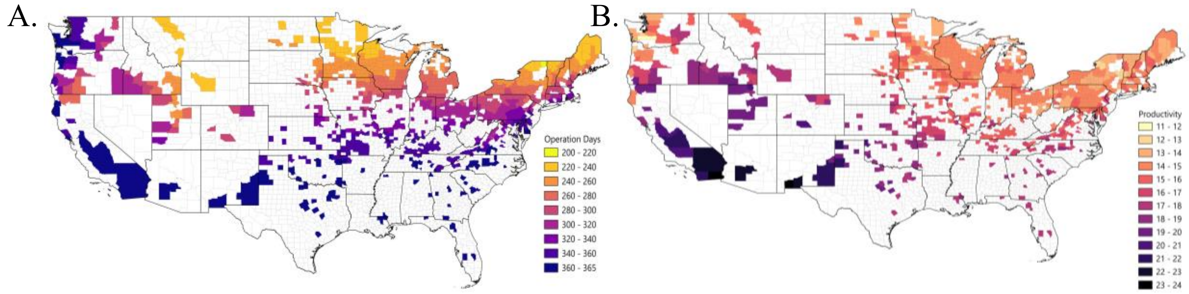

Figure A5. A) Estimated operational days for filtered EPA anaerobic lagoon sites, based on the frequency of freezing events. B) Estimated algal productivity for the same filtered candidate anaerobic lagoon sites, based on global horizontal irradiance and algal light-use efficiency. White areas in both panels represent regions with missing data, zero wastewater flow, or sites excluded during EPA-based anaerobic lagoon filtering [4].

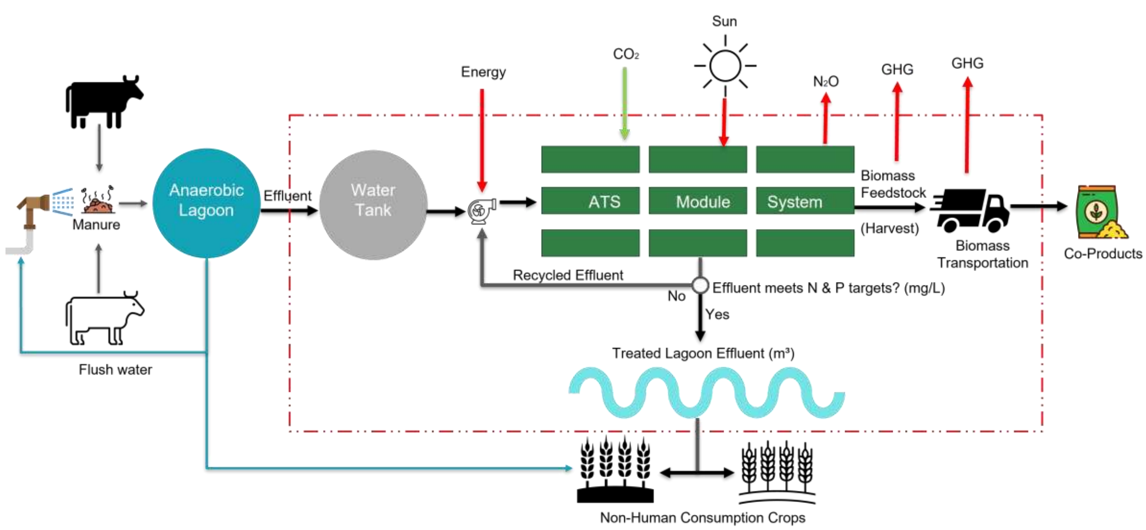

Figure A6. Diagram of algal turf scrubber (ATS) treatment process. ATS treatment system includes the flow-way and pumps to support the recirculation process. The total volume of the pond enters the ATS system and recycles. The ATS system is scaled to complete the required cycles in a day.

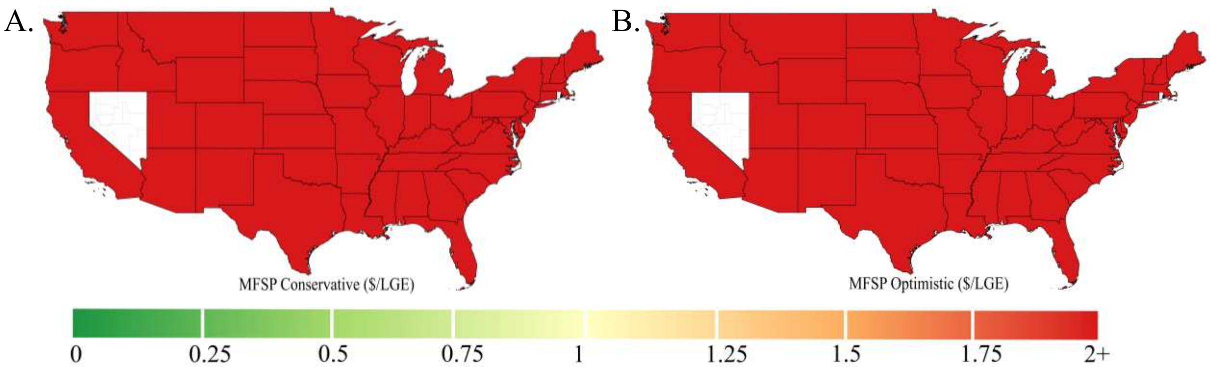

Figure A7. Spatial distribution of renewable diesel MFSP from ATS biomass A) conservative and B) optimistic cost scenarios. Values are reported in $ LGE^{-1} and exclude nutrient-credit credits. Red areas exceed the target MFSP of $0.98 LGE^{-1}, while white areas indicate locations where MFSP could not be evaluated due to the absence of qualifying dairy-lagoon facilities.

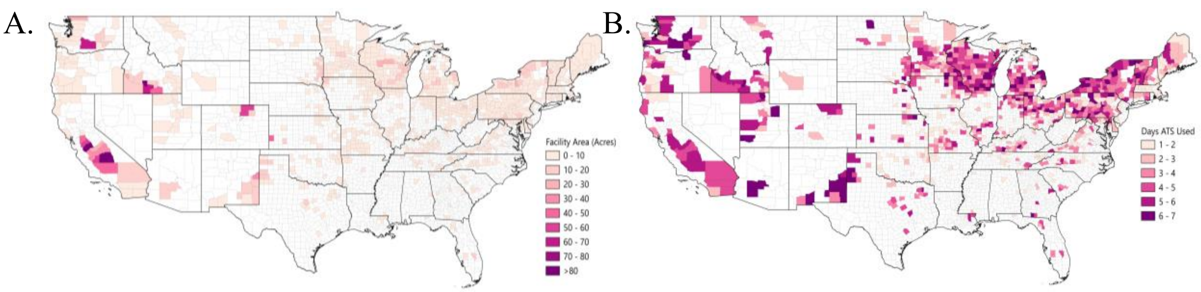

Figure A8. A) Average ATS facility area, expressed in acres, required at each anaerobic lagoon site across the continental United States (CONUS). B) Number of days that water must remain recirculating through the ATS system to achieve nutrient reduction at each site. White areas in both maps represent regions with missing data, zero wastewater flow, or sites excluded from the analysis.

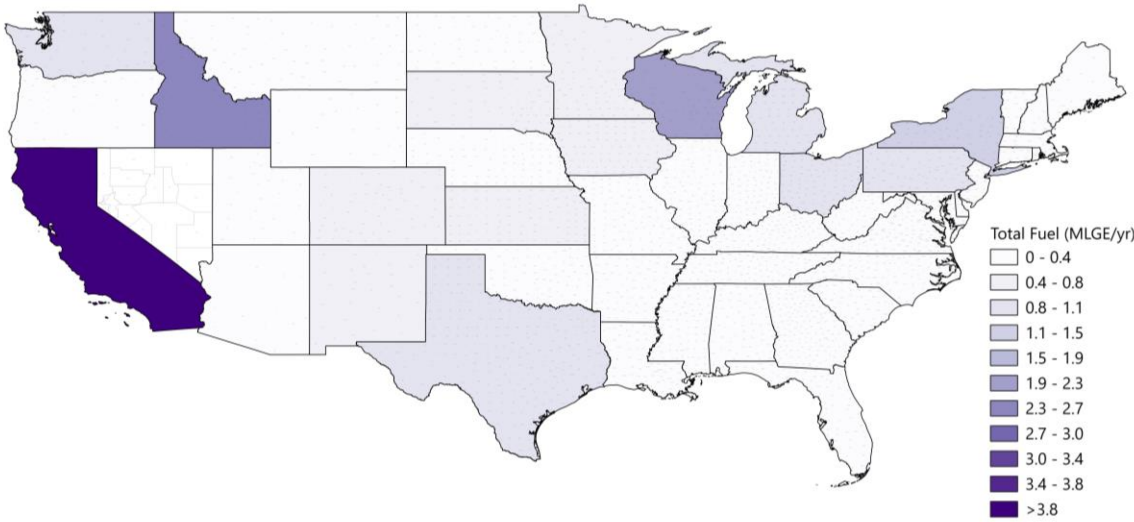

Figure A9. Total fuel production attributed to the centralized biorefinery assigned to each state, expressed in million liter gasoline equivalents per year (MLGE yr^{-1}). Each biorefinery was located in the county selected as the state-level hub, defined by the highest dairy concentration and corresponding feedstock availability. White areas represent regions with missing data, zero wastewater flow, or states with no qualifying anaerobic lagoon sites in the analysis.

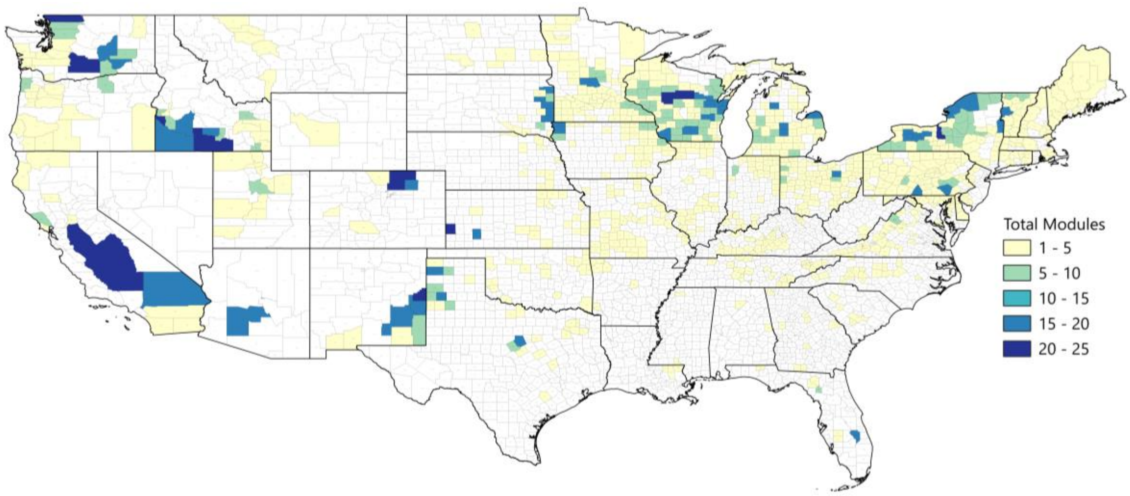

Figure A10. Estimated number of ATS modules required per facility under a regular modular layout to improve nutrient uptake through serial operation.

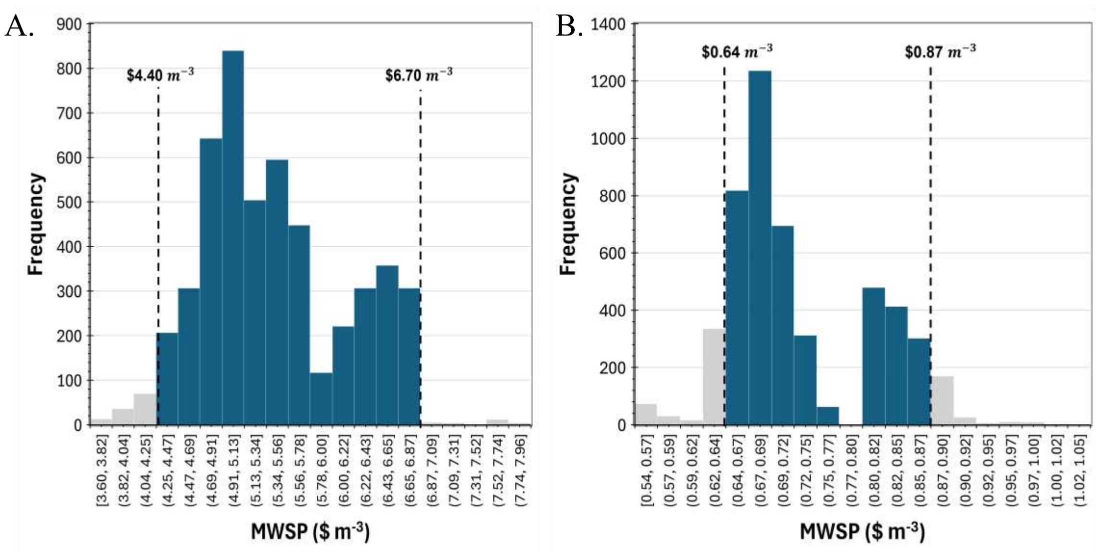

Figure A11. Monte Carlo histograms for MWSP under conservative and optimistic scenarios. A) Conservative MWSP. B) Conservative MWSP. Blue bars show the central 90% of the simulated output distribution, defined by the 5th and 95th percentiles, whereas gray bars indicate the lower and upper tails outside this interval.

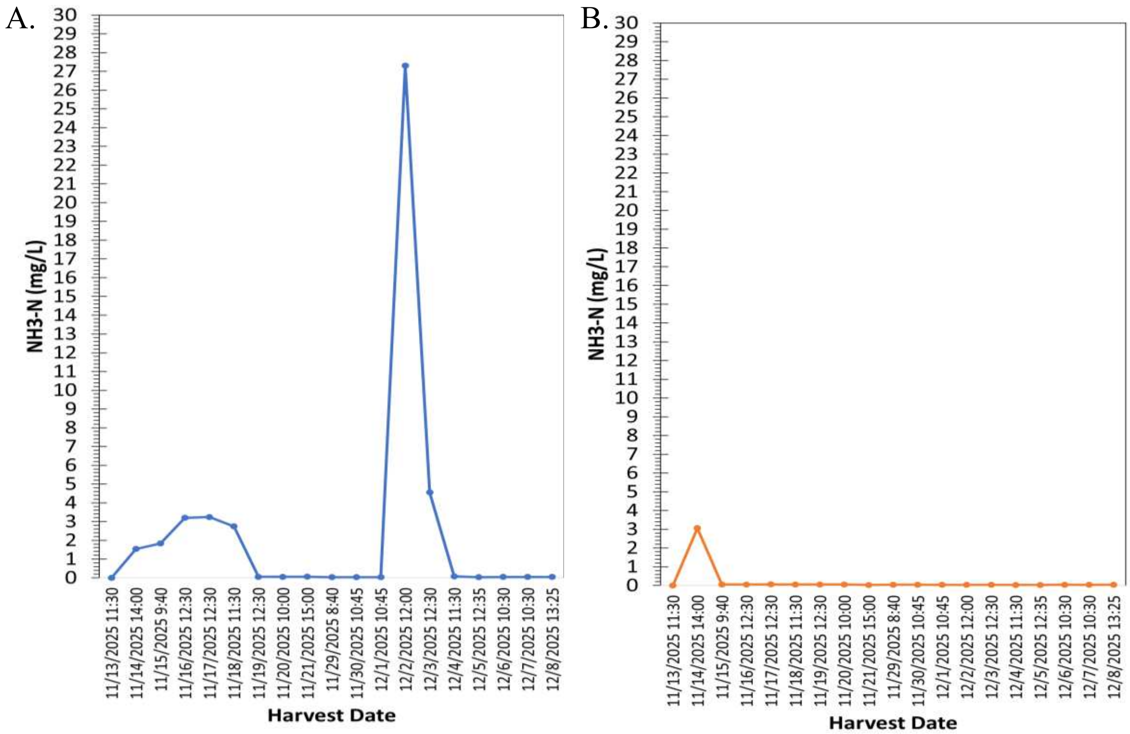

Figure A12. Algal ammonia uptake observed in the (A) 100 ppm TN flow-way and (B) 50 ppm TN flow-way at CSU.

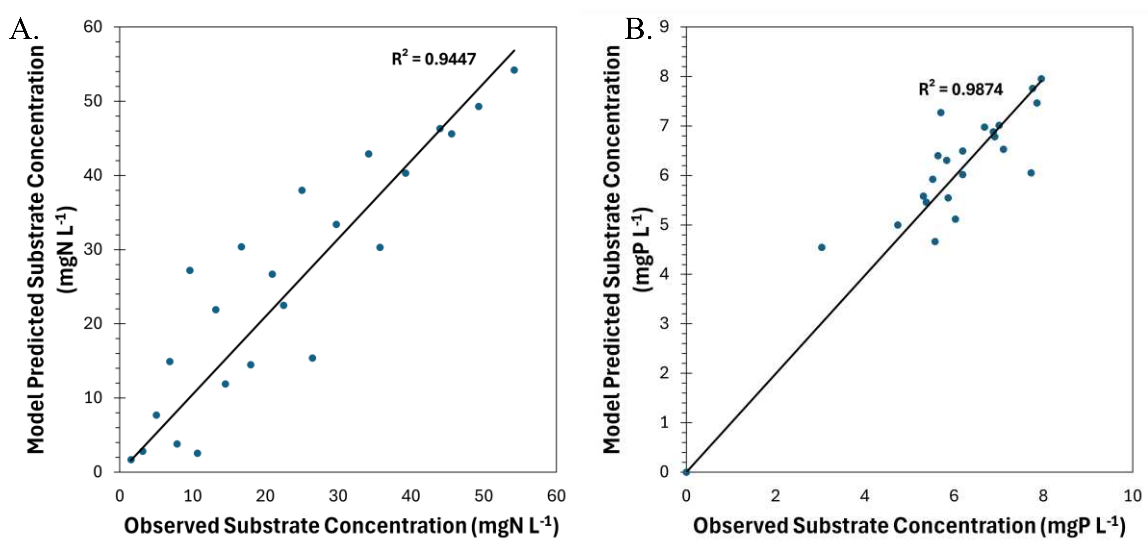

Figure A13. Correlation between observed laboratory substrate concentrations and model-predicted concentrations using the Monod biokinetic model for A) nitrogen and B) phosphorus. R^2 values of 0.9447 for nitrogen and 0.9874 for phosphorus.

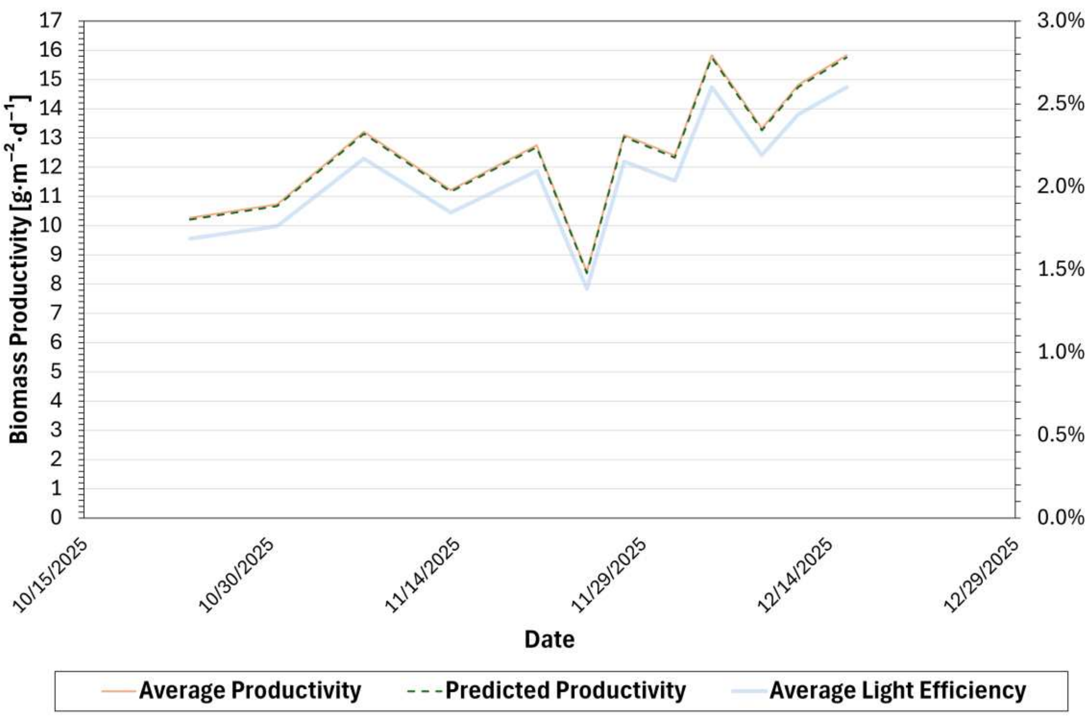

Figure A14. Experimental light-use efficiency obtained at the Energy Institute at Colorado State University for an algae flow-way operated with 100ppm TN and 10ppm TP at an average 708.33 µmol/(m2*s).

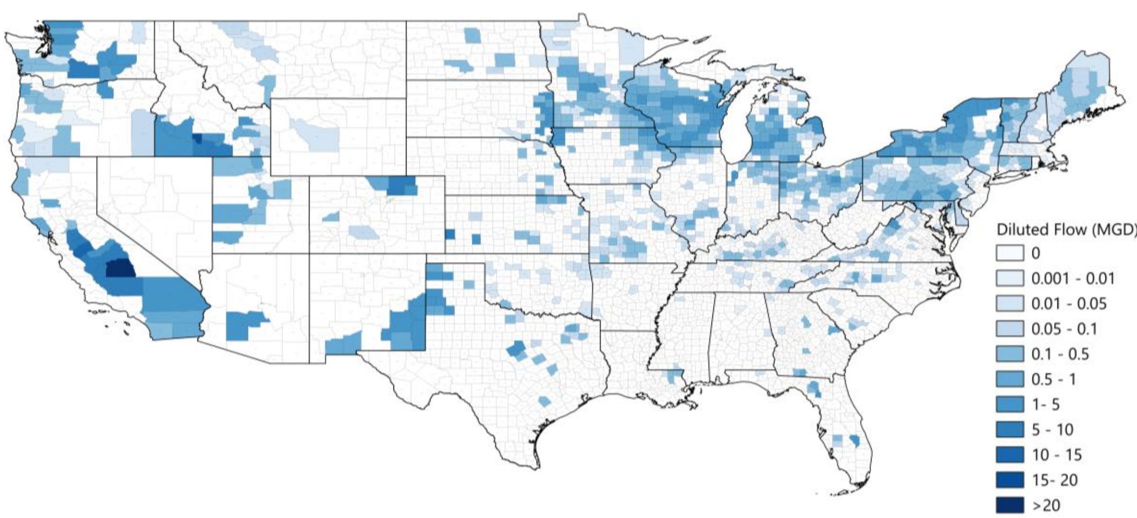

Figure A15. Diluted daily water entering the ATS system per dairy facility after adjusting anaerobic lagoon effluent to 100ppm TN. Flow is expressed in MGD.

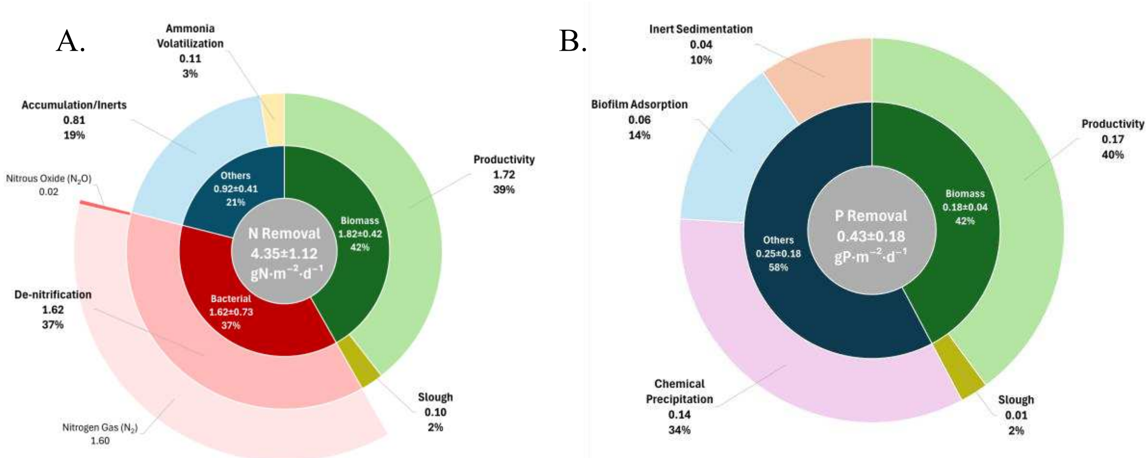

Figure A16. A) Breakdown of N removal rates under high-nutrient loading conditions. B) Breakdown of P removal rates under high-nutrient loading conditions. Biomass and slough fractions in both panels were obtained experimentally under 100 ppm TN and 10 ppm TP for freshwater algae, whereas the remaining component fractions were assigned based on literature values.

A.2 Nutrient Targets

Crop-based effluent nutrient targets were developed to estimate nitrogen (N) and phosphorus (P) concentrations in treated water that would be consistent with agronomic reuse under state-specific irrigation conditions. First, crop nutrient requirements were compiled as areal application rates in lb/ac for each crop scenario as established by Clark et al. 39 [6]. Then, average state irrigation application rates, expressed in acre-feet per acre (acre-ft/ac) by USDA IWMS [7], were used to convert these areal nutrient loads into equivalent concentration targets in mg/L. The final target table presented in this study was generated using the procedure described below.

Phosphorus conversion

Phosphorus recommendations were originally reported as P_2O_5 and were converted to elemental phosphorus (P) before calculating concentration targets. The conversion factor used was:

$$P = P_2O_5 \times 0.4364 \; [\boldsymbol{Eq. A. 2. 1}]$$

where 0.4364 is the fraction of elemental P contained in P_2O_5. This conversion gives phosphorus loading in lb P/ac.

Irrigation rate

State-level irrigation application was expressed as:

$$I = \text{acre-ft/ac} \; [\boldsymbol{Eq. A. 2. 2}]$$

where I represents the average irrigation volume applied per acre in each state. These values were used to convert nutrient application rates from a land basis to a water concentration basis.

Conversion from lb/ac to mg/L

To convert nutrient loads from lb/ac to mg/L, the following unit conversions were used:

$$1 \text{ lb} = 453{,}592.37 \text{ mg}$$
$$1 \text{ acre-ft} = 1{,}233{,}480 \text{ L}$$

Thus,

$$\frac{453{,}592.37}{1{,}233{,}480} = 0.3677$$

where 0.3677 is the conversion factor used to express lb/ac per acre-ft/ac as mg/L.

Nitrogen target calculation

Nitrogen targets were calculated as:

$$TN_{target} = \frac{N_{load}}{I} \times 0.3677 \; [\boldsymbol{Eq. A.2.3}]$$

where:

- TN_{target}= nitrogen target concentration in mg N/L
- N_{load}= crop nitrogen requirement in lb N/ac
- I= state irrigation rate in acre-ft/ac

Phosphorus target calculation

Phosphorus targets were calculated by first converting P_2O_5 to elemental P, then converting to concentration:

$$TP_{target} = \frac{P_{2O_5,load} \times 0.4364}{I} \times 0.3677 \; [\boldsymbol{Eq. A.2.4}]$$

where:

- TP_{target}= phosphorus target concentration in mg P/L
- $P_{2O_5,load}$= crop phosphorus requirement in lb P_2O_5/ac
- 0.4364= conversion from P_2O_5 to elemental P
- I= state irrigation rate in acre-ft/ac
- 0.3677= conversion from lb/ac per acre-ft/ac to mg/L

The final state-level target values for each crop and production scenario were obtained using these equations and will be provided for reference.

A.3 Process Model Equations

Equation A1. Productivity Calculation

$$\text{prod} = \text{GHI} * \frac{86400\text{ s}}{1\text{ day}} * \frac{1\text{ kJ}}{1000\text{J}} * \text{GHI\_PAR} * \text{light}_{\text{eff}} * \frac{1}{\text{energy density}} \quad [\boldsymbol{Eq.A.3.1}]$$

Where:

prod = productivity of biomass; g m^{-2} day^{-1}

GHI = global horizontal irradiance; W m^{-2}

GHI_PAR = 0.458; (kJ m^{-2} day^{-1} PAR) (kJ m^{-2} day^{-1} $GHI)^{-1}$

$\text{light}_{\text{eff}}$ = 2.71; %

energy density = 22; kJ g^{-1}

Equation A2. Dairy Cows in Anaerobic Lagoons Calculation

$$N_{AL,c} = N_{dairy,c}, * \left(\frac{f_{AL,s}}{100}\right) \quad [\boldsymbol{Eq.A.3.2}]$$

where $N_{AL,c}$ is the number of dairy cows (head) assigned to anaerobic lagoons per county (c), $N_{dairy,c}$ is the total number of dairy cows reported for each county c(head), and $f_{AL,s}$is the state-level percentage of dairy manure managed in anaerobic lagoons (%).

Equation A3. Dairy Water Flow available for ATS Treatment

$$Q_{w,c} = N_{AL,c}(Q_m)\left(\frac{453.6g}{1\ lb}\right)\left(\frac{1}{\rho_w}\right) \quad [\boldsymbol{Eq.A.3.3}]$$

where $Q_{w,c}$ is the daily water flow available for ATS treatment in county c (L day^{-1}), $N_{AL,c}$is the number of dairy cows assigned to anaerobic lagoons (head), Q_m is the daily manure/effluent flow factor from NRCS Table 4-16 (REFERENCE), 234 lb cow^{-1} day $^{-1}$, and ρ_w is the assumed water density 1000 g L^{-1}. This conversion gives approximately 106 cow^{-1} day $^{-1}$.

Equation A4. Batch water volume and annual treated flow

Because the ATS system was modeled as a closed batch-recirculation system, only one day of lagoon effluent was introduced into the treatment tank per batch. After the valve was closed, this same water volume was recirculated through the ATS system for the selected treatment time.

$$V_{batch,c} = Q_{w,c}(1 \text{ day})$$

$$N_{batch,yr} = \frac{365}{t_R} \; [\boldsymbol{Eq.A.3.4a}]$$

$$V_{treated,yr,c} = V_{batch,c} N_{batch,yr} \; [\boldsymbol{Eq.A.3.4b}]$$

where $V_{batch,c}$ is the water volume treated per batch (L batch^{-1}), $N_{batch,yr}$ is the number of batches treated per year, t_R is the batch recirculation or treatment time (days batch^{-1}), and $V_{treated,yr,c}$ is the total annual treated water volume (L yr^{-1}). The term $365/t_R$ accounts for the number of treatment batches per year.

Equation A5. Annual total Nitrogen Loading under batch recirculation

$$TN_c = N_{AL,c}(Q_m)\left(\frac{453.6g}{1\,lb}\right)\left(\frac{1kg}{1000g}\right)\left(\frac{TKN_{wb}}{100}\right)\left(\frac{365}{t_r}\right) \; [\boldsymbol{Eq.A.3.5}]$$

where TN_c is the annual total nitrogen loading in county c (kg N yr^{-1}), $N_{AL,c}$is the number of dairy cows assigned to anaerobic lagoons (head), Q_m is the daily manure/effluent flow factor from NRCS Table 4-16 [8], 234 lb cow^{-1} day $^{-1}$, TKN_{wb} is the total Kjeldahl nitrogen content on a wet-basis percentage (%wb) and 365 converts the daily loading to annual loading and $t_R$is the batch recirculation or treatment time (days batch^{-1}).

Equation A6. Annual total Nitrogen Loading under batch recirculation

$$TP_c = N_{AL,c}(Q_m)\left(\frac{453.6g}{1\,lb}\right)\left(\frac{1kg}{1000g}\right)\left(\frac{P_{wb}}{100}\right)\left(\frac{365}{t_r}\right) \; [\boldsymbol{Eq.A.3.6}]$$

where TP_c is the annual total phosphorus loading in county c (kg P yr^{-1}), $N_{AL,c}$ is the number of dairy cows assigned to anaerobic lagoons (head), Q_m is the daily manure/effluent flow factor from NRCS Table 4-16 [8], 234 lb cow^{-1} day $^{-1}$, P_{wb} is the phosphorus content on a wet-basis percentage (%wb) and 365 converts the daily loading to annual loading and $t_R$is the batch recirculation or treatment time (days batch^{-1}).

Equation A7. Electricity Equation

$$\text{pumping power} = \left(\text{flow} * \text{pump}_{\text{energy}} * \frac{24\text{ hr}}{1\text{ day}}\right) - \left(\frac{\text{flow}}{\text{cycles}} * \text{pump}_{\text{energy}} * \frac{24\text{ hr}}{1\text{ day}}\right) \; [\boldsymbol{Eq.A.3.7}]$$

Where:

pumping power = electricity use of the algal turf scrubber to pump water through the system

flow = $\mathrm{MLD} * 10^6 * \frac{1\ \mathrm{m}^3}{1000\ \mathrm{L}}\ \frac{1\ \mathrm{day}}{24\ \mathrm{hr}} * \mathrm{cycles}$; $m^3\ hr^{-1}$

MLD = design flow of the WWTP in million liters per day

cycles = Number of times the volume of water needs to pass through the system in one day

$\mathrm{pump}_{\mathrm{energy}}$ = 0.0267kWh m^{-3}

A.4 Media Recipe

Table A4.1. Media recipe.

NaNO3 (mg/L)	75.94
NH4Cl (mg/L)	47.79
KH2PO4 (mg/L)	22.00
MgSO4*7H2O (mg/L)	202.73
CaCl2*2H2O (mg/L)	146.70
NaHCO3 (mg/L)	82.61
L1 Bigelow Trace Metals (mL)	0.10
L1 Bigelow vitamin solution (mL)	0.05
Water Volume (L)	454.25L

A.5 Sensitivity and Uncertainty Analysis

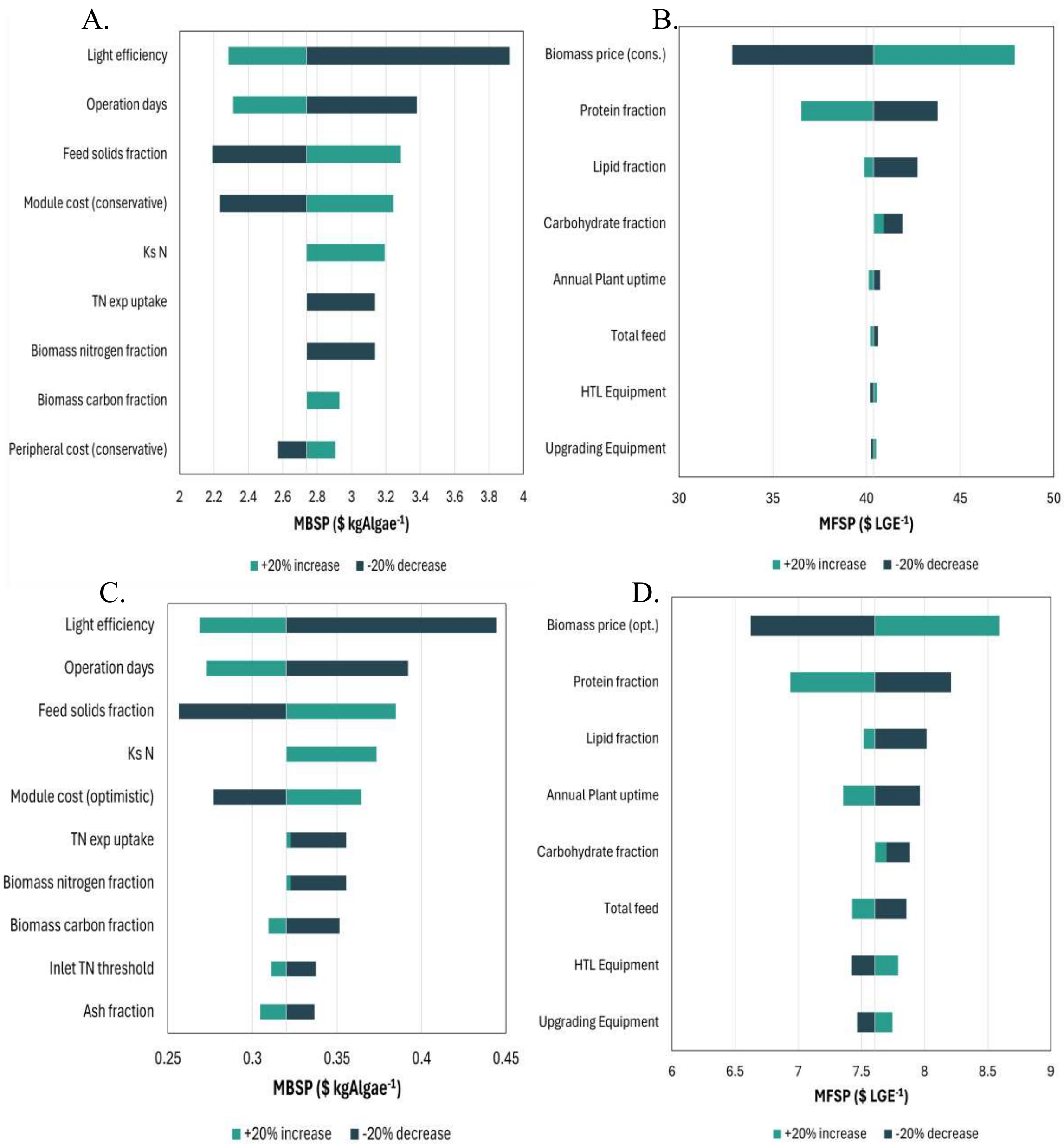

Figure A5.1. Tornado plots of the most sensitive parameters affecting cultivation MBSP and HTL MFSP under ± 20% variation from the base case. A) Conservative MBSP. B) Conservative MFSP. C) Optimistic MBSP. D) Optimistic MFSP. The top row corresponds to the conservative scenario and the bottom row to the optimistic scenario.

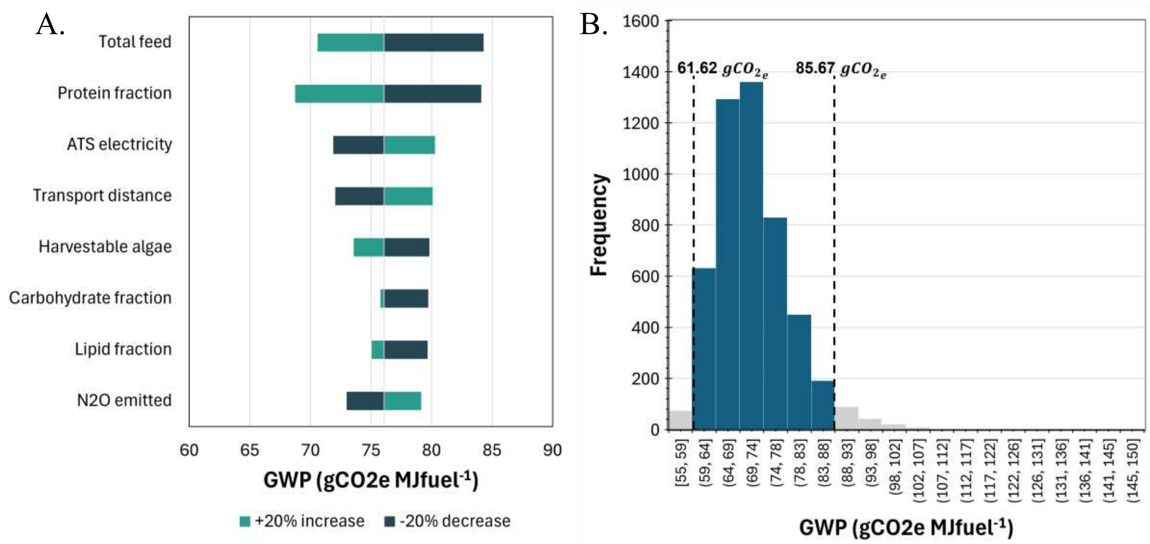

Figure A5.2 Sensitivity and Monte Carlo analysis of GWP for the Weld County representative case. A) Tornado plot showing the effect of ± 20% variation in the most sensitive parameters on net GWP. B) Monte Carlo histogram of simulated GWP values. The blue region represents the central 90% prediction interval, bounded by the 5th (P5) and 95th (P95) percentiles of the simulated output distribution, while the gray tails represent values outside this interval. Dashed vertical lines indicate the P5 and P95 bounds.

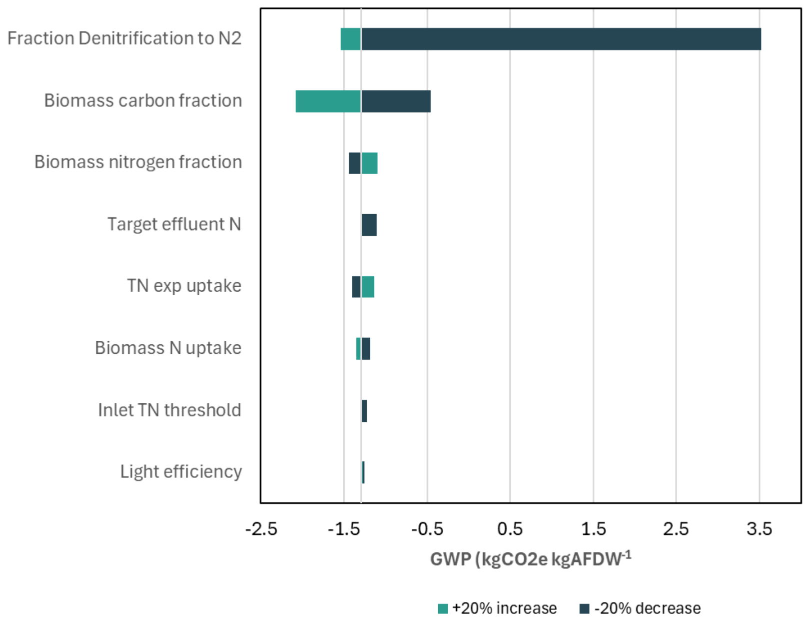

Figure A5.3 Sensitivity analysis of cultivation-stage GWP for the Weld County case, excluding harvest and feedstock transportation requirements. Bars show the change in GWP resulting from a ±20% variation in the most sensitive cultivation parameters.

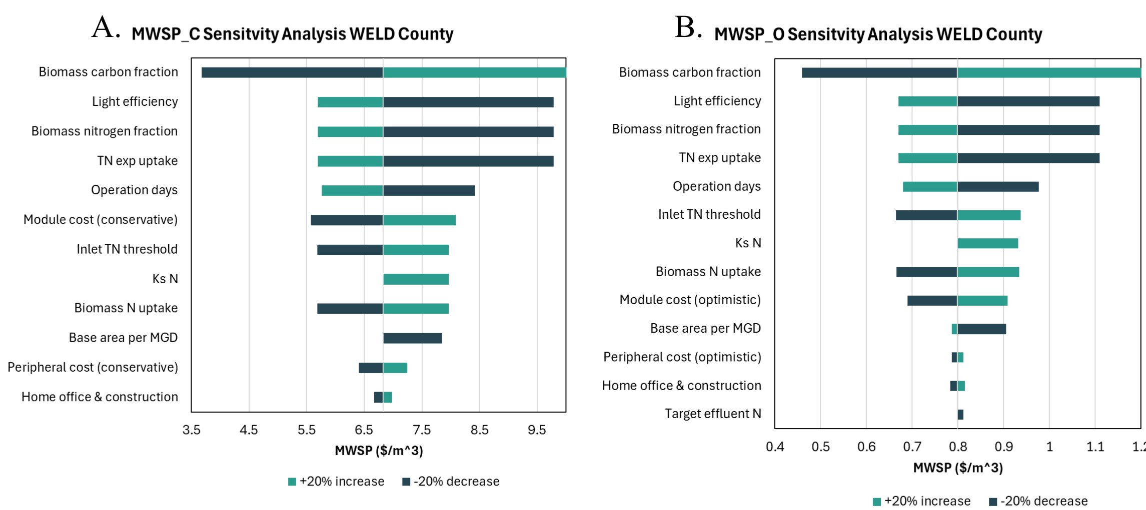

Figure A5.4 Sensitivity analysis of minimum wastewater selling price (MWSP) for the Weld County cultivation model. A) Conservative cost case. B) Optimistic cost case. Bars show the response of MWSP to a ±20% variation in the most sensitive cultivation parameters.

A.6 1st order growth model

To obtain the required nutrient and productivity data for model development, controlled experiments were performed using the media presented in table A3. Two experimental flow-ways were operated at different nitrogen concentrations: one at 50 ppm and the other at 100 ppm of nitrogen. Both systems maintained a nitrogen-to-phosphorus ratio of 10:1, consistent for anaerobic lagoons. This resulted in phosphorus concentrations of 5 ppm and 10 ppm, respectively. A ramping diurnal light cycle of 16 hours was simulated to replicate outdoor conditions. Light intensity peaked for one hour at 2000 $\mu mol\ m^{-2}\ s^{-1}$, while the remaining hours followed a ramp-up and ramp-down pattern designed to approximate a natural daylight cycle. The trapezoidal area method was used to determine the average daily photosynthetically active radiation (PAR) expressed as 708.33 $\mu mol\ m^{-2}\ s^{-1}$ or a GHI of 338.42 $W\ m^{-2}$. A first-order growth model using Equation A.1 with PAR as the primary variable was applied and solving for light efficiency for each week's productivity calculating an overall average. Similar approaches (Banks et al., 2023) [4] have been shown to effectively describe the growth of photosynthetic microorganisms under light-limited conditions.

For this analysis, the laboratory flow-way operated at 50 ppm N was used, yielding a calculated light-use efficiency of 2.71% $\pm$ 0.57%. This value is consistent with the reported outdoor light-use efficiency of 2.80%, associated with a maximum algal productivity of 25 $g\ m^{-2}\ day^{-1}$ in large-scale algal cultivation systems in New Mexico (Banks et al. (2023)) [4]. Future work will incorporate a second-order temperature-dependent growth model to account for the influence of temperature on algal productivity. Such models consider cardinal temperatures that define the minimum, optimum, and maximum temperature ranges for algal growth based on Rosso et al. (1993) [9].

A.7 Nutrient Uptake rates

Removal rates were calculated by subtracting the final concentration from the initial concentration and dividing by the number of days the ATS operated between harvest events, resulting in nutrient removal expressed in mgN day^{-1} and mgP day^{-1}. These values were then normalized by the harvested algal cultivation area to obtain removal rates in units of mass per area per day. The resulting values were averaged across all experimental cycles to obtain representative removal rates.

$$\Delta S = S_i - S_f$$

$$R_s = \frac{\Delta S * V}{A * t}$$

Table 1. Variables used for determining experimental Nitrogen and Phosphorus removal rates

Variable	Definition	Units
ΔS	Substrate removed	mg L^{-1}
S_i	initial substrate concentration	mg L^{-1}
S_f	final substrate concentration	mg L^{-1}
R_s	substrate removal rate	mg substrate m^{-2} day^{-1}
A	algal cultivation area	m^2
V	Water tank Volume	L
t	time between harvest events	days
$R_{biomass}$	Substrate removal rate due to algal assimilation	mg substrate m^{-2} day^{-1}
R_{others}	Substrate removal rate due to other processes	mg substrate m^{-2} day^{-1}

$f_{substrate}$	Mass fraction of nutrient in biomass	mg substrate mg biomass^{-1}

For P, chemical precipitation was assigned an approximate weighting factor of 35% based on HRAP studies reporting that P precipitation under high-pH conditions can account for a substantial share of P removal, in some cases approximately half of the total removed P [37], [38], [39]. The remaining non-assimilatory P was apportioned to biofilm adsorption/filtration (approximately 15%) and minor inert sedimentation (approximately 10%) as literature-supported allocation assumptions representing particulate retention and settling within the algal-biofilm matrix.

A.8 Biokinetic Parameters Derivation

Microbial growth kinetics have been extensively studied to describe how microorganisms utilize nutrients and convert them into biomass [10]. Monod demonstrated that microbial growth rates depend on substrate availability and proposed a mathematical formulation relating the specific growth rate of microorganisms to substrate concentration [10]. This relationship, commonly known as the Monod model, was originally inspired by the enzyme kinetics described by Michaelis and Menten, who analyzed how reaction rates depend on substrate concentration in enzymatic systems [10]. Microbial interactions play an important role in algal systems. Algae are eukaryotic microorganisms whose growth depends on nutrient availability, light exposure, and environmental conditions such as pH and oxygen concentration [10]. In water environments, other microorganisms, including bacteria and cyanobacteria (often referred to as blue-green algae), may compete for nutrients or influence algal growth [17]. In high-nutrient systems, improper environmental control can lead to unfavorable conditions such as elevated pH and nutrient competition, which may shift community composition and inhibit algal productivity [18]. The influent of this study originates from an anaerobic lagoon, where it initially contains limited dissolved oxygen, but the designed outdoor ATS promotes oxygen production as sunlight and atmospheric exposure allow photosynthesis to occur [10].

TN concentrations were measured using the HACH TNTplus vial test 835/836, while TP was quantified using HACH TNTplus vial test 843/844. NH_3 concentrations were analyzed using TNTplus vial test 830, and nitrite (NO_2) was monitored using TNTplus vial test 839. When nutrient concentrations exceeded the analytical range of the reagent, samples were diluted at a 1:10 ratio and the measured value was corrected by the dilution factor. NH_3 and NO_2 measurements were primarily used to evaluate nitrate (NO_3^-) consumption and potential bacterial activity within the ATS system. The measured nutrient concentrations time interval between samples, total water volume and flow-way cultivation area were then used to evaluate the kinetic behavior described by Eq. 13. Detailed analytical procedures, concentration ranges, and reagent-specific methods are available in the official HACH TNTplus methodology documentation.

Monod Growth Model is expressed as [10]:

$$\mu = \mu_{max} \frac{S}{K_s + S} - b \; [\boldsymbol{Eq.1}]$$

where:

Table 2. Monod biokinetics model variables

Variable	Definition	Units
μ	specific microbial growth rate	day^{-1}
μmax	maximum specific growth rate	day^{-1}

S	substrate concentration	mg L^{-1}
K_s	half-saturation constant	mg L^{-1}
b	endogenous decay coefficient	day^{-1}
t	time	days
r_{ut}	substrate utilization rate	mg L^{-1} day^{-1}
r_{max}	maximum substrate utilization rate	mg L^{-1} day^{-1}
Y	biomass yield coefficient	mg biomass mg $substrate^{-1}$
X_a	active biomass concentration	mg biomass L^{-1}
$\hat{q}$	maximum specific substrate utilization rate	mg substrate mg $biomass^{-1}$ day^{-1}
$r_{max}^{(V)}$	volumetric maximum substrate utilization rate	mg substrate L^{-1} day^{-1}
$r_{max}^{(A)}$	areal maximum substrate utilization rate	mg substrate m^{-2} day^{-1}

Consumption of substrate due to microbial activity can be expressed as:

$$\frac{dS}{dt} = -r_{ut}\ [\boldsymbol{Eq. 2}]$$

Substrate utilization rate is related to microbial growth through the yield coefficient:

$$r_{ut} = \frac{\mu}{Y} X_a\ [\boldsymbol{Eq. 3}]$$

Substituting the Monod growth expression into the substrate utilization equation gives:

$$r_{ut} = \frac{1}{Y} * \left(\mu_{max} \frac{S}{K_s + S} - b\right) * X_a\ [\boldsymbol{Eq. 4}]$$

For simplification, the decay term is often neglected when its effect is small relative to microbial growth:

$$b = 0$$

Additionally, the **maximum specific substrate utilization rate** can be defined as:

$$\hat{q} = \frac{\mu_{max}}{Y} \ [\boldsymbol{Eq.5}]$$

Or equivalently

$$\mu_{max} = \hat{q}Y \ [\boldsymbol{Eq.6}]$$

Substituting **[Eq. 6]** in **[Eq. 4]:**

$$r_{ut} = \frac{1}{Y} * \left(\hat{q}Y \frac{S}{K_s + S}\right) * X_a$$

which simplifies to

$$r_{ut} = \hat{q} * X_a \left(\frac{S}{K_s + S}\right) \ [\boldsymbol{Eq.7}]$$

The maximum substrate utilization rate can therefore be defined as

$$r_{max} = \hat{q} * X_a \ [\boldsymbol{Eq.8}]$$

Substituting **Eq. 8** into **Eq.7** and **Eq. 2** results in

$$\frac{dS}{dt} = -r_{max} \left(\frac{S}{K_s + S}\right) \ [\boldsymbol{Eq.9}]$$

To determine the change in substrate concentration over time, the equation is integrated between $S_1$and S_2:

$$\int_{t_1}^{t_2} dt = -\frac{1}{r_{max}} \int_{S1}^{S_2} \frac{K_s + S}{S} dS \; [\boldsymbol{Eq. 10}]$$

Solving the integral gives

$$t_2 - t_1 = -\frac{1}{r_{max}} \left[(S_2 - S_1) + K_s \ln\left(\frac{S_2}{S_1}\right) \right] \; [\boldsymbol{Eq. 11}]$$

The parameter r_{max} obtained from the integrated Monod expression is initially expressed on a volumetric basis. To express r_{max} in terms of surface productivity (gS m^{-2} day^{-1}), the reactor volume and surface area defined in the experimental setup were incorporated. Additionally, the negative sign can be absorbed into the integration limits to avoid confusion when interpreting substrate removal.

Since substrate concentration is given in units of mass per volume, the volumetric maximum substrate utilization rate has units of

$$r_{max}^{(V)} = \frac{mgS}{day} * \frac{1}{L}$$

However, for the present ATS system, nutrient removal performance is more appropriately expressed on a surface area basis, since algal growth occurs over the channel surface. Therefore, an areal maximum substrate utilization rate is defined as

$$r_{max}^{(A)} = \frac{mgS}{day} * \frac{1}{m^2}$$

The relationship between both forms is obtained through the surface area-to-volume ratio of the system:

$$r_{max}^{(V)} = r_{max}^{(A)} * \frac{A}{V} \; [\boldsymbol{Eq. 12}]$$

where:

- A= surface area of the ATS channel (m^2)
- V= water volume in the system (L)

Substituting this expression into the integrated Monod equation gives

$$t_2 - t_1 = \frac{V}{A * r_{max}^{(A)}} \left[(S_1 - S_2) + K_s \ln \left(\frac{S_1}{S_2} \right) \right] \; [\boldsymbol{Eq. 13}]$$

This form is more convenient for interpreting laboratory data in terms of nutrient removal per unit area of reactor surface.

For application to the laboratory data:

Table 3. Variables needed for determining Monod biokinetics model with experimental data

Variable	Definition	Units
t_1	Start of the harvest period or initial sampling time	day
t_2	Subsequent sampling time	day
V	Water volume in the system	L
A	Affective surface area of the ATS channel	m^2
S_1	Initial substrate concentration at time t_1	mg L^{-1}
S_2	Substrate concentration at time t_2	mg L^{-1}
K_s	Half-saturation constant	mg L^{-1}
$r_{max}^{(A)}$	areal maximum substrate utilization rate	mg substrate m^{-2} day^{-1}

This formulation allows the Monod model to be directly fitted to the experimental nutrient removal data collected throughout the cultivation period.

After obtaining the kinetic expression, the remaining unknown parameters were K_s and $r_{max}^{(A)}$. These parameters were estimated by fitting the model to the experimental data using a sum of squared errors (SSE) minimization approach [11]. For each observation, the theoretical time interval predicted by the kinetic model was compared with the measured time interval:

$$(t_2 - t_1)_{exp} \approx (t_2 - t_1)_{model}$$

The objective function was defined as

$$SSE = \sum_{i=1}^{n} \left(t_i^{(exp)} - t_i^{(model)} \right)^2 = 0 \;\; [\boldsymbol{Eq.\,14}]$$

and the values of K_s and $r_{max}^{(A)}$ were selected such that the SSE was minimized and in literature range.

A.9 Water and ATS mass Balance derivation

Bio-Kinetics and Mass Balances

Overall Mass balance

The general mass balance for any conserved quantity in the system can be written as

$$Accumulation = Input - Output - Reaction \ \ [\boldsymbol{Eq.1}]$$

This framework will be applied separately to the water tank and the ATS modules.

Water Flow Mass Balance

For the water balance, the reaction term is assumed to be zero as the algae in the system is periphytic, meaning organisms attach to surfaces and that no biomass will grow suspended in the water [10], [12], [13].

Therefore,

$$Accumulation = Input - Output + 0 \ [\boldsymbol{Eq.2}]$$

- **Substrate Mass balance in the tank**

For dissolved nutrients (nitrogen or phosphorus), the substrate mass balance can be written as

$$\frac{dm}{dt} = \dot{m}_{in} - \dot{m}_{out} \ [\boldsymbol{Eq.3}]$$

where

$$m = V_T * S \ [\boldsymbol{Eq.4}]$$

and

$$\dot{m} = Q * S \ [\boldsymbol{Eq.5}]$$

Variable	Definition	Units
m	substrate mass	Kg
$\dot{m}$	substrate mass rate	Kg day^{-1}
V_T	tank volume	L
S	substrate concentration	kg L^{-1}
$Q = Q_w$	water flow rate	L day^{-1}
k_w	tank recirculation rate	cycles day^{-1}

$$\frac{d(V_T S)}{dt} = Q_{in}S_{in} - Q_{out}S_{out} \; [\boldsymbol{Eq.6}]$$

Assumptions:

- Evaporation losses were considered negligible for the system but can be incorporated using the rates reported by Quiroz et al. (2021) [14].
- Constant tank/pond volume

$$Q_{in} = Q_{out} = Q_w \; [\boldsymbol{Eq.7}]$$

And

$$V_T = constant$$

the equation becomes

$$V_T \frac{dS}{dt} = Q_w S_{in} - Q_w S_{out} \; [\boldsymbol{Eq.8}]$$

Dividing by V_T

$$\frac{dS}{dt} = \frac{Q_w}{V_T}(S_{in} - S_{out})[\boldsymbol{Eq.9}]$$

We define the tank recirculation rate as:

$$\frac{Q_w}{V_T} = k_w = cycles\ day^{-1}\ [\boldsymbol{Eq.10}]$$

Which is the inverse of the hydraulic retention time.

Thus,

$$\frac{dS}{dt} = k_w(S_{in} - S_{out})\ [\boldsymbol{Eq.11}]$$

- **Solving the First-Order Ordinary Differential Equation (1st ODE)**

Rearranging

$$\frac{dS}{dt} + k_w S_{out} = k_w S_{in}\ [\boldsymbol{Eq.12}]$$

The homogeneous solution is

$$\frac{dS}{dt} + k_w S_{out} = 0\ [\boldsymbol{Eq.13}]$$

Solving the differential equation,

$$S_h(t) = Ce^{-k_w t}\ [\boldsymbol{Eq.14}]$$

The particular solution is,

$$S_p = S_{in}\ [\boldsymbol{Eq.15}]$$

The general solution is defined as

$$S(t) = S_h(t)\ + S_p [\boldsymbol{Eq.16}]$$

Thus, the general solution becomes,

$$S(t) = Ce^{-k_w t} + S_{in}\ [\boldsymbol{Eq.17}]$$

Applying the initial condition

$$at\ t = 0;\ S_{t=0} = S_0$$

gives

$$C = S_0 - S_{in}$$

and therefore

$$S(t) = (S_0 - S_{in})e^{-k_w t} + S_{in} [\boldsymbol{Eq. 18}]$$

Discrete Time Formulation

For numerical implementation, the analytical solution can be written in step form.

$$t_{n+1} = t_n + \Delta t \ [\boldsymbol{Eq. 19}]$$

$$\Delta t = t_{n+1} - t_n \ [\boldsymbol{Eq. 20}]$$

$$S_{(t=t_{n+1})} = S_{(t_n+\Delta t)} = S_{n+1} \ [\boldsymbol{Eq. 21}]$$

So,

$$\text{at } t = t_n; \ S_{(t=n)} = S_n \ [\boldsymbol{Eq. 22}]$$

$$S_n = Ce^{-k_w t_n} + S_{in}$$

$$C = (S_n - S_{in})e^{k_w t_n}$$

General solution at time step,

$$S_{(t=t_{n+1})} = (S_n - S_{in})e^{k_w t_n}e^{-k_w t_{n+1}} + S_{in} [\boldsymbol{Eq. 23}]$$

$$S_{(t=t_{n+1})} = (S_n - S_{in})e^{-k_w (t_{n+1} - t_n)} + S_{in} [\boldsymbol{Eq. 24}]$$

Substituting,

$$S_{n+1} = (S_n - S_{in})e^{-k_w \Delta t} + S_{in} \ [\boldsymbol{Eq. 25}]$$

ATS Mass Balance

The algal turf scrubber is modeled as a surface-attached biological reactor where substrate removal occurs through algal uptake [10], [12], [13].

Applying the general mass balance and assuming steady conditions within the ATS module (as the algae is attached):

$$0 = Input - Output - Reaction[\boldsymbol{Eq.26}]$$

thus

$$0 = Q_w S_{in} - Q_w S_{out} - V_{ATS}(r_{ut})[\boldsymbol{Eq.27}]$$

Where

$$V_{ATS} = A_{ATS} * h_{ATS}[\boldsymbol{Eq.28}]$$

Variable	**Definition**	**Units**
h_{ATS}	ATS thickness	m
A_{ATS}	ATS surface area	m^2
V_{ATS}	ATS volume	L
Productivity	Biomass Productivity	mg biomass m^{-2} day^{-1}
$f_{substrate}$	Mass fraction of nutrient in biomass	mg substrate · mg $biomass^{-1}$
J_s	Substrate Uptake Flow	mg substrate m^{-3} day^{-1}
J_{max}	Maximum Substrate Uptake Flux	mg substrate m^{-2} day^{-1}

- **Monod Kinetics for substrate uptake**

$$r_{ut} = \hat{q} * X_a \left(\frac{S}{K_s + S}\right) \; [\boldsymbol{Eq.7\ Section\ A7}]$$

Where we define a similar constant to Eq.8 but with a different meaning,

We define J_s as the substrate uptake flux:

$$J_s = \hat{q} * X_a \; [\boldsymbol{Eq.29}]$$

Relation between substrate uptake flow and biomass characteristics:

$$J_s = \hat{q} * X_a = \frac{mg_{substrate}}{mg_{biomasss} * day} * \frac{mg_{biomass}}{A_{ATS} * h_{ATS}} = \frac{1}{h_{ATS}} * \frac{mg_{biomass}}{A_{ATS} * day} * \frac{mg_{substrate}}{mg_{biomass}}$$

$$J_s = \frac{1}{h_{ATS}} * Productivity * f_{substrate} \; [\boldsymbol{Eq.30}]$$

$$J_{max} = Productivity * f_{substrate} \; [\boldsymbol{Eq.31}]$$

$$J_s = \frac{1}{h_{ATS}} * J_{max} \; [\boldsymbol{Eq.32}]$$

J_{max} =maximum substrate uptake flux based on productivity and % of substrate in biomass

Substituting into the ATS balance

$$0 = Q_w S_{in} - Q_w S_{out} - A_{ATS} * h_{ATS} * \frac{1}{h_{ATS}} * J_{max} \frac{S}{K_s + S} \; [\boldsymbol{Eq.33}]$$

Rearranging

$$Q_w(S_{in} - S_{out}) = A_{ATS} * J_{max} \frac{S_{out}}{K_s + S_{out}} \; [\boldsymbol{Eq.34}]$$

Coupling Tank and ATS

The tank and ATS are connected through recirculation.

The tank output concentration (S_n) becomes the inlet to the ATS

The tank input concentration (S_{in}) becomes the output of the ATS

$$S_n = Actual\ concentration\ in\ the\ tank$$

$$\boldsymbol{S_n = S_{out,tank} = S_{in,ATS}} \; [\boldsymbol{Eq.35}]$$

$$\boldsymbol{S_{in} = S_{in,Tank} = S_{out,ATS}} \; [\boldsymbol{Eq.36}]$$

Thus

$$\boldsymbol{Q_w\left(S_n - S_{out,ATS}\right) = A_{ATS} * J_{max}\frac{S_{out,ATS}}{K_s + S_{out,ATS}}\ [Eq.37]}$$

Finally, the tank concentration update becomes

$$\boldsymbol{S_{n+1} = (S_n - S_{out,ATS})e^{-k_w \Delta t} + S_{out,ATS}[Eq.38]}$$

which provides the coupled **hydraulic–biokinetic model** used to simulate nutrient removal in the system. This gives us a two variable, two equation system which the model is going to solve by doing time steps in a defined interval.

A.10 Nutrient Credit Lookup Function

The nutrient-credit scenario was used to estimate the nitrogen (N) and phosphorus (P) credit values required for the ATS-to-renewable-diesel pathway to reach diesel price parity. The target fuel selling price was defined as:

$$FSP_{target} = 0.98\ \$\ LGE^{-1}$$

where FSP_{target} is the target fuel selling price based on the EIA diesel price converted from \$ GGE^{-1} to \$ LGE^{-1} [15].

The total nutrient credit required to reach the target fuel selling price was solved using the discounted cash-flow model:

$$NPV(FSP_{target}, Fuel_{yr}, Credit_{needed}, CAPEX, OPEX, CoProducts, Feedstock) = 0$$

where NPV is the net present value of the fuel pathway, , $Fuel_{yr}$ is the annual fuel production, $Credit_{needed}$ is the annual nutrient-credit revenue required to reach the target fuel selling price, CAPEX is the capital expenditure, OPEX is the operating expenditure, CoProducts represents co-product credits, and Feedstock represents the ATS biomass feedstock cost.

The base N and P credit rates were obtained from the selected Limb-based nutrient-credit level [5]:

$$r_N, Limb\ (\$\ kg\ N^{-1})$$

$$r_P, Limb\ (\$\ kg\ P^{-1})$$

where r_N,Limb and r_P,Limb are the base N and P credit rates from the selected Limb et al. nutrient-credit level.

The annual credit value expected from the Limb-based rates was calculated as:

$$Credit_{Limb} = r_N, Limb\ N_{rem} + r_P, Limb\ P_{rem}$$

where $Credit_{Limb}$ is the annual nutrient-credit value based on the original Limb-based credit rates (\$ yr^{-1}), N_{rem} is the annual nitrogen removed by the ATS system (kg N yr^{-1}), and P_{rem} is the annual phosphorus removed by the ATS system (kg P yr^{-1}).

A scaling factor was then calculated to preserve the Limb-based N:P credit allocation while adjusting the total credit value to the amount required by the TEA:

$$s = \frac{Credit_{needed}}{Credit_{Limb}}$$

where s is the dimensionless scaling factor, $Credit_{needed}$ is the annual credit revenue required to reach FSP_{target}, and $Credit_{Limb}$ is the annual credit value obtained using the original Limb-based rates.

The scaled N and P credit rates were then calculated as:

$$r_N, needed = s * r_N, Limb$$

$$r_P, needed = s * r_P, Limb$$

where $r_N, needed$ and $r_P, needed$ are the N and P credit rates required for the pathway to reach the target fuel selling price.

Finally, the required annual nutrient credit was expressed as:

$$Credit_{needed} = r_N, needed\ N_{rem} + r_P, needed\ P_{rem}$$

This approach preserved the relative N:P credit structure from the Limb-based framework while scaling the total nutrient-credit value to the level required for the ATS-to-renewable-diesel pathway to reach 0.98 \$ LGE^{-1}.

A.11 Monte Carlo design parameters

For the MBSP we chose the 5 most sensitive parameters described in the sensitivity analysis: light efficiency, K_sN, N uptake, the cost to make a module and the amount of algal solids in the wet biomass. For light-use efficiency, the baseline value used in the model is the laboratory-derived value of 2.71%, with a standard deviation of 0.271%. Literature reviews indicate that microalgae may theoretically reach approximately 8–10% solar-to-biomass efficiency, whereas a more realistic practical value is closer to 4.5% [23]. Because the baseline already represents current system performance, this parameter was only allowed to vary upward, with a 20% security bound, corresponding to a maximum value of 3.25%, to represent technological improvement rather than deterioration of the present system.

For the N half-saturation constant, the baseline value used in the model is the laboratory-derived value of 13.40 mg N L^{-1} and the standard deviation was 1.340 mg N L^{-1}. This value falls within the range reported in the literature for comparable green microalgae systems [19], [20], [21]. Since the calibrated model value lies within this reported range, a standard deviation equal to 10% of the baseline value is considered reasonable, together with a 20% security bound to avoid unrealistic extreme samples. For N uptake, the laboratory baseline was used in the model 4.35 g N m^{-2} d^{-1} and the standard deviation was 0.435 g N m^{-2} d^{-1}. This choice was based on a 10% uncertainty assumption supported by high-uptake ATS literature, where relative deviations of approximately 8–10% were observed in the highest N recovery cases [22]. A 20% security bound was then applied to constrain the parameter to a realistic range around the experimental baseline.

For feed solids fraction, the baseline value used in the model is the experimental value of 0.20 with a standard deviation of 0.02. This baseline is consistent with the wet slurry condition commonly assumed for algal HTL feedstocks, where 20 wt% solids is frequently used as a representative dewatered feed condition, and the broader HTL literature often discusses slurry concentrations in the range of approximately 15–25 wt% solids [24]. Therefore, a standard deviation equal to 10% of the baseline value, together with a 20% security bound, is considered reasonable for Monte Carlo sampling. For module cost, uncertainty was treated asymmetrically. In the conservative case, the baseline multiplier was 1.0 and the standard deviation was 0.1. This parameter was only allowed to move downward, representing the assumption that future technological improvement would reduce costs relative to the current baseline. In the optimistic case, the baseline multiplier was also 1.0 and the standard deviation was 0.1, but the parameter was only allowed to move upward, reflecting the assumption that the DeRose-based optimistic values [16] are already highly favorable and that more realistic future performance would be expected to deviate upward from those best-case assumptions. In both cases, a 20% security bound is applied to keep the sampled values within a plausible range around the selected baseline.

Based on these assumptions, the Monte Carlo analysis for the MBSP in Weld County yields a mean MBSP of \$2.14 kg wet algae slurry^{-1}, a standard deviation of \$0.27 kg wet algae slurry^{-1} under the conservative case, and a mean MBSP of \$0.29 kg wet algae slurry^{-1} with a standard deviation of \$0.03 kg wet algae slurry^{-1} under the optimistic case. In addition, the simulated total algae feedstock had a mean of 4,135,977.865 kg wet algae slurry yr^{-1} and a standard deviation of 813,735.883 kg wet algae slurry yr^{-1}. For MWSP, the Monte Carlo analysis yielded a mean of \$5.42 m^{-3} with a standard deviation of \$0.72 m^{-3} under the conservative case, and a mean of \$0.72 m^{-3} with a standard deviation of \$0.08 m^{-3} under the optimistic case (see Appendix Figure A11).

For the MFSP, the five most sensitive parameters identified in the sensitivity analysis are selected: MBSP, total wet algae feedstock, and the protein, carbohydrate, and lipid fractions. For MBSP and total wet algae feed, the input distributions were taken from the cultivation Monte Carlo analysis in Weld County and then scaled to Colorado using the corresponding Colorado baseline values. This produced a conservative MBSP mean of \$2.72 kg $algae^{-1}$ with a standard deviation of \$0.34 kg $algae^{-1}$, an optimistic MBSP mean of \$0.38 kg $algae^{-1}$ with a standard deviation of \$0.04 kg $algae^{-1}$, and a total algae feed mean of 7,961,712.04 kg algae yr^{-1} with a standard deviation of 1,566,432.65 kg algae yr^{-1}. Further details on the scaling procedure is provided in Appendix section A10.

For protein, carbohydrate, and lipid fractions, triangular distributions are used based on literature-informed lower, most likely, and upper values. For protein, a minimum of 0.46, a mode based on the lab-composition of 0.516, and a maximum of 0.56 are selected based mainly on Valdez et al. (2014) [25] and Gong et al. (2019) [22]. Valdez et al. reported 50% protein for *Scenedesmus* sp., while Gong et al. reported a measured batch composition of 45.7% protein and also cited literature values of approximately 50–56% for *Scenedesmus obliquus*.

For carbohydrates, a minimum of 0.20, a mode based on the lab-composition of 0.310, and a maximum of 0.40 are selected mainly based on Valdez et al. (2014) [25] and Wang et al. (2013) [20]. Valdez et al. reported 31% carbohydrate for *Scenedesmus* sp., which is essentially the same as the baseline value used in this study, while Wang et al. shows that *Scenedesmus dimorphus* can shift toward carbohydrate-rich biomass depending on cultivation strategy, supporting the use of a higher upper bound.

For lipids, a minimum of 0.052, a mode based on Valdez of 0.080, and a maximum of 0.15 are selected. The minimum was kept at the laboratory composition value, since it represents the lowest value observed in this case. The mode was shifted to 0.080 based on Valdez et al. (2014), who reported 8% lipid for *Scenedesmus* sp., while the maximum of 0.15 was selected as a conservative upper bound supported by Gong et al. (2019), who cited values of approximately 12–14% lipid for *Scenedesmus obliquus*. Triangular distributions are selected for protein, carbohydrate, and lipid fractions, whereas MBSP and total wet algae feed retained the cultivation-model-based distributions. Combining these distribution types within the same Monte Carlo framework is valid, since the final output distribution reflects the combined effect of all sampled inputs.

Based on these assumptions, the Monte Carlo analysis for the MFSP in Colorado yielded a mean MFSP of \$30.36 LGE^{-1} with a standard deviation of \$3.81 LGE^{-1} under the conservative case, and a mean MFSP of \$6.69 LGE^{-1} with a standard deviation of \$0.61 LGE^{-1} under the optimistic case.

A.12 References

[1] U.S. Department of Agriculture, "2022 Census Dairy Data," 2022. [Online]. Available: https://quickstats.nass.usda.gov/

[2] Environmental Protection Agency, "Concentrated animal feeding operations," Jun. 2025, [Online]. Available: https://www.ecfr.gov/current/title-40/chapter-I/subchapter-D/part-122/subpart-B/section-122.23

[3] "Agricultural Waste Characteristics," USDA NRCS, Washington, D.C, Chapter 4, 2008.

[4] A. B. Banks, P. H. Chen, C. Quiroz-Arita, R. W. Davis, and J. C. Quinn, "Geographically-resolved evaluation of the economic and environmental services from renewable diesel derived from attached algae flow-ways across the United States," *Algal Res*, vol. 72, p. 103100, May 2023, doi: 10.1016/J.ALGAL.2023.103100.

[5] B. J. Limb, J. C. Quinn, A. Johnson, R. B. Sowby, and E. Thomas, "The potential of carbon markets to accelerate green infrastructure based water quality trading," *Commun Earth Environ*, vol. 5, no. 1, p. 185, Apr. 2024, doi: 10.1038/s43247-024-01359-x.

[6] J. Clark, J. Gerwing, and R. Gelderman, "Fertilizer Recommendations Guide," 2005.

[7] Environmental Protection Agency, "IWMS - Entire Farm Data Irrigation Rates," vol. Table 7, 2023.

[8] "Agricultural Waste Characteristics," USDA NRCS, Washington, D.C, Chapter 4, 2008.

[9] L. Rosso, J. R. Lobry, and J. P. Flandrois, "An Unexpected Correlation between Cardinal Temperatures of Microbial Growth Highlighted by a New Model," *Journal of Theoretical Biology*, vol. 162, no. 4, pp. 447–463, Jun. 1993, doi: 10.1006/jtbi.1993.1099.

[10] B. E. Rittmann and P. L. McCarty, *Environmental Biotechnology: Principles and Applications*, 2nd Edition. New York: McGraw-Hill Education, 2020. [Online]. Available: https://www.accessengineeringlibrary.com/content/book/9781260441604

[11] H.-Y. Kim, "Statistical notes for clinical researchers: simple linear regression 1 – basic concepts," *Restor Dent Endod*, vol. 43, no. 2, p. e21, Apr. 2018, doi: 10.5395/rde.2018.43.e21.

[12] R. W. Davis, "Attached Periphytic Algae Production & Analysis," *DOE Bioenergy Technologies Office (BETO) 2021 Project Peer Review*, Mar. 2021.

[13] J. Hoffman, R. C. Pate, T. Drennen, and J. C. Quinn, "Techno-economic assessment of open microalgae production systems," *Algal Research*, vol. 23, pp. 51–57, Apr. 2017, doi: 10.1016/j.algal.2017.01.005.

[14] D. Quiroz, J. M. Greene, J. McGowen, and J. C. Quinn, "Geographical assessment of open pond algal productivity and evaporation losses across the United States," *Algal Research*, vol. 60, p. 102483, Dec. 2021, doi: 10.1016/j.algal.2021.102483.

[15] U.S. Energy Information Administration (EIA), "U.S. Gasoline and Diesel Retail Prices." Accessed: Mar. 05, 2026. [Online]. Available: https://www.eia.gov/dnav/pet/pet_pri_gnd_dcus_nus_w.htm

[16] K. DeRose, C. DeMill, R. W. Davis, and J. C. Quinn, "Integrated techno economic and life cycle assessment of the conversion of high productivity, low lipid algae to renewable fuels," *Algal Research*, vol. 38, p. 101412, Mar. 2019, doi: 10.1016/j.algal.2019.101412.

[17] D. F. Toerien and C. H. Huang, "Algal growth prediction using growth kinetic constants," *Water Research*, vol. 7, no. 11, pp. 1673–1681, Nov. 1973, doi: 10.1016/0043-1354(73)90135-8.

[18] A. Thornton, "Modeling and optimization of algae growth," *CASA Report*, vol. 1059, Jan. 2010.

[19] A. S. Zurano, C. G. Serrano, F. G. Acién-Fernández, J. M. Fernández-Sevilla, and E. Molina-Grima, "Modelling of photosynthesis, respiration, and nutrient yield coefficients in Scenedemus almeriensis culture as a function of nitrogen and phosphorus," *Appl Microbiol Biotechnol*, vol. 105, no. 19, pp. 7487–7503, Oct. 2021, doi: 10.1007/s00253-021-11484-8.

[20] L. Wang, Y. Li, M. Sommerfeld, and Q. Hu, "A flexible culture process for production of the green microalga Scenedesmus dimorphus rich in protein, carbohydrate or lipid," *Bioresource Technology*, vol. 129, pp. 289–295, Feb. 2013, doi: 10.1016/j.biortech.2012.10.062.

[21] Y. Gong *et al.*, "Microalgae Scenedesmus sp. as a potential ingredient in low fishmeal diets for Atlantic salmon (Salmo salar L.)," *Aquaculture*, vol. 501, pp. 455–464, Feb. 2019, doi: 10.1016/j.aquaculture.2018.11.049.

[22] W. Mulbry, S. Kondrad, C. Pizarro, and E. Kebede-Westhead, "Treatment of dairy manure effluent using freshwater algae: Algal productivity and recovery of manure

nutrients using pilot-scale algal turf scrubbers," *Bioresource Technology*, vol. 99, no. 17, pp. 8137–8142, Nov. 2008, doi: 10.1016/j.biortech.2008.03.073.

[23] L. Xin, H. Hong-ying, G. Ke, and S. Ying-xue, "Effects of different nitrogen and phosphorus concentrations on the growth, nutrient uptake, and lipid accumulation of a freshwater microalga Scenedesmus sp.," *Bioresource Technology*, vol. 101, no. 14, pp. 5494–5500, Jul. 2010, doi: 10.1016/j.biortech.2010.02.016.

[24] E. Sforza, M. Pastore, E. Barbera, and A. Bertucco, "Respirometry as a tool to quantify kinetic parameters of microalgal mixotrophic growth," *Bioprocess Biosyst Eng*, vol. 42, no. 5, pp. 839–851, May 2019, doi: 10.1007/s00449-019-02087-9.

[25] P. J. Valdez, V. J. Tocco, and P. E. Savage, "A general kinetic model for the hydrothermal liquefaction of microalgae," *Bioresource Technology*, vol. 163, pp. 123–127, Jul. 2014, doi: 10.1016/j.biortech.2014.04.013.